

2015

IRF-5-dependent signaling restricts Orthobunyavirus dissemination to the central nervous system

Jose Luiz Proenca-Modena

Washington University School of Medicine in St. Louis

Jennifer L. Hyde

Washington University School of Medicine in St. Louis

Renata Sesti-Costa

Washington University School of Medicine in St. Louis

Tiffany Lucas

Washington University School of Medicine in St. Louis

Amelia K. Pinto

Washington University School of Medicine in St. Louis

See next page for additional authors

Follow this and additional works at: http://digitalcommons.wustl.edu/open_access_pubs

Recommended Citation

Proenca-Modena, Jose Luiz; Hyde, Jennifer L.; Sesti-Costa, Renata; Lucas, Tiffany; Pinto, Amelia K.; Richner, Justin M.; Gorman, Matthew J.; Lazear, Helen M.; and Diamond, Michael S., "IRF-5-dependent signaling restricts Orthobunyavirus dissemination to the central nervous system." *The Journal of Virology*,. 1-46. (2015).
http://digitalcommons.wustl.edu/open_access_pubs/4370

Authors

Jose Luiz Proenca-Modena, Jennifer L. Hyde, Renata Sesti-Costa, Tiffany Lucas, Amelia K. Pinto, Justin M. Richner, Matthew J. Gorman, Helen M. Lazear, and Michael S. Diamond

1 **IRF-5-dependent signaling restricts Orthobunyavirus dissemination to the central**
2 **nervous system**

3
4 Jose Luiz Proenca-Modena^{a,e}, Jennifer L. Hyde^a, Renata Sesti-Costa^{b,f}, Tiffany Lucas^a,
5 Amelia K. Pinto^a, Justin M. Richner^a, Matthew J. Gorman^b, Helen M. Lazear^{a,g}, and Michael
6 S. Diamond^{a,b,c,d}

7
8 Departments of Medicine^a, Pathology & Immunology^b, and Molecular Microbiology^c, Center
9 for Human Immunology and Immunotherapy Programs^d, Washington University School of
10 Medicine, St Louis, MO, USA. Department of Genetics, Evolution and Bioagents^e, Institute of
11 Biology, University of Campinas (UNICAMP), Campinas, SP, Brazil. Department of
12 Biochemistry and Immunology^f, University of São Paulo (USP), Ribeirão Preto School of
13 Medicine, SP, Brazil. Department of Microbiology and Immunology, University of North
14 Carolina School of Medicine, Chapel Hill, NC, USA^g

15
16 **Corresponding author:** Michael Diamond, MD, PhD. Departments of Medicine, Molecular
17 Microbiology, Pathology & Immunology. Center for Human Immunology & Immunotherapy
18 Programs Washington University School of Medicine. 660 South Euclid Ave, St Louis MO
19 63110. Phone: +1-314-362-2842, e-mail: diamond@wusm.wustl.edu

20
21 **Short Title:** Neuropathogenesis of OROV is restricted by IRF-5

22 **Figures: 12; Tables: 2**

23

24

25 **ABSTRACT**

26 Interferon (IFN)-regulatory factor 5 (IRF-5) is a transcription factor that induces
27 inflammatory responses after engagement and signaling by pattern recognition receptors. To
28 define the role of IRF-5 during bunyavirus infection, we evaluated Oropouche virus (OROV)
29 and La Crosse virus (LACV) pathogenesis and immune responses in primary cells and in
30 mice with gene deletions in *Irf3*, *Irf5*, and *Irf7* or *Irf5* alone. Deletion of *Irf3*, *Irf5*, and *Irf7*
31 together resulted in uncontrolled viral replication in the liver and spleen, hypercytokinemia,
32 extensive liver injury, and an early death phenotype. Remarkably, deletion of *Irf5* alone
33 resulted in meningoencephalitis and death on a more protracted timeline, one to two weeks
34 after initial OROV or LACV infection. The clinical signs in OROV-infected *Irf5*^{-/-} mice were
35 associated with abundant viral antigen and TUNEL-positive cells in several regions of the
36 brain. Circulating dendritic cell (DC) subsets in *Irf5*^{-/-} mice had higher levels of OROV RNA *in*
37 *vivo* yet produced lower levels of type I IFN compared to WT cells. This result was supported
38 by data obtained *in vitro*, since a deficiency of IRF-5 resulted in enhanced OROV infection
39 and diminished type I IFN production in bone marrow-derived DCs. Collectively, these
40 results indicate a key role for IRF-5 in modulating the host antiviral response in peripheral
41 organs that controls bunyavirus neuroinvasion in mice.

42

43

44 **IMPORTANCE**

45 Oropouche virus (OROV) and La Crosse virus (LACV) are orthobunyaviruses that
46 are transmitted by insects and cause meningitis and encephalitis in subsets of individuals in
47 the Americas. Recently, we demonstrated that components of the type I interferon (IFN)
48 induction pathway, particularly the regulatory transcription factors IRF-3 and IRF-7, have key
49 protective roles during OROV infection. However, the lethality in *Irf3^{-/-} Irf7^{-/-}* (DKO) mice
50 infected with OROV was not as rapid or complete as observed in *Ifnar^{-/-}* mice, indicating that
51 other transcriptional factors associated with an IFN response contribute to antiviral immunity
52 against OROV. Here, we evaluated bunyavirus replication, tissue tropism, and cytokine
53 production in primary cells and mice lacking IRF-5. We demonstrate an important role for
54 IRF-5 in preventing neuroinvasion and the ensuing encephalitis caused by OROV and
55 LACV.

56

57

58 **INTRODUCTION**

59 The interferon (IFN) regulatory factor (IRF) family of transcription factors has a
60 central role in regulating innate immune cell development and responses (1). Several IRF
61 family members (e.g., IRF-1, IRF-3, IRF-5, and IRF-7) are present in the cytoplasm in an
62 inactive form and then phosphorylated after pattern recognition receptor engagement and
63 signaling. These events facilitate nuclear translocation, binding to DNA promoter elements,
64 and induction of antiviral and proinflammatory genes that modulate immunity (2). Canonical
65 IFN induction pathways that are regulated by Toll-like (TLR) and RIG-I-like (RLR) receptors
66 converge on activation of IRF-3 and IRF-7 (3).

67 IRF-5 acts downstream of the TLR–MyD88 and RLR-MAVS signaling pathways, via
68 a TRAF6- and IRAK1-dependent mechanism, to induce expression of proinflammatory
69 cytokines, including interleukin-6 (IL-6), IL-12, and TNF- α (4). IRF-5 is expressed
70 constitutively in several hematopoietic cells, including B cells, monocytes, macrophages
71 (M ϕ), and dendritic cell (DC) subsets (5, 6). IRF-5 regulates differentiation of lymphoid cells
72 and innate immune responses, but also is implicated in oncogenesis and apoptosis (7, 8).
73 During B cell development, IRF-5 regulates expression of Blimp-1, a protein required for the
74 formation of immunoglobulin-secreting plasma cells. As a consequence, *Irf5*^{-/-} mice have
75 increased numbers of CD19⁺B220⁻ cells and reduced plasma cell expansion and isotype
76 switching in response to antigens or pathogens (9-11). A deficiency of IRF-5 also resulted in
77 reduced IFN- α , IFN- β , and IL-6 production by TLR-7- and TLR-9-stimulated DCs or IL-6
78 production by B cells (9, 12), and this was associated with resistance to shock syndrome
79 induced by unmethylated CpG DNA and LPS (4). *Irf5* alleles with enhanced promoter activity
80 are linked to autoimmune disorders in humans, including systemic lupus erythematosus,
81 rheumatoid arthritis, Sjögren's syndrome, multiple sclerosis, and inflammatory bowel disease
82 (13-16).

83 Recent studies have illustrated the importance of IRF-5 function in antiviral immunity
84 (17). After MAVS signaling, IRF-5 acts coordinately with IRF-3 and IRF-7 to regulate type I
85 IFN responses in myeloid DCs after West Nile virus (WNV) infection (18). In addition, IRF-5

86 shapes the early innate immune response against WNV in the draining lymph node (11). An
87 IRF-5 deficiency was associated with lower levels of proinflammatory cytokines,
88 chemokines, and activated immune cells in lymphoid tissues within two days of WNV
89 infection (11). *Irf5*^{-/-} mice also had a mildly blunted WNV-specific antibody response, with
90 fewer antigen-specific memory B cells and long-lived plasma cells (11).

91 Oropouche virus (OROV) is an arthropod-transmitted, enveloped, negative-sense
92 orthobunyavirus of the family *Bunyaviridae* that has caused periodic outbreaks of a
93 debilitating febrile illness in South America (19). Oropouche fever is the second most
94 frequent arthropod-transmitted viral disease in Brazil, and more than 500,000 cases have
95 been confirmed in Brazil, Peru, Trinidad, Panama, and Suriname (19-21). OROV infection
96 can progress to meningitis and/or encephalitis in some patients (22-24). Despite its clinical
97 importance, little is known about the factors that determine OROV dissemination into the
98 central nervous system (CNS).

99 A recent study in mice with targeted gene deletions provided insight into mechanisms
100 of innate immune restriction of OROV infection (25). The host type I IFN antiviral response is
101 essential for controlling OROV infection, as mice lacking interferon- α/β receptor (*Ifnar*^{-/-}) or
102 signaling molecules and transcription factors involved in IFN production (e.g. *Mavs*^{-/-}, *Irf3*^{-/-},
103 or *Irf7*^{-/-}) sustained high levels of virus replication in the liver and spleen (25). However, *Irf3*^{-/-}
104 *Irf7*^{-/-} double knockout (DKO) mice were not as vulnerable to OROV or La Crosse virus
105 (LACV, a second orthobunyavirus) infection compared to *Ifnar*^{-/-} mice (25), suggesting that
106 additional transcriptional factors regulated IFN-dependent antiviral immunity.

107 To define the role of IRF-5 to restrict OROV infection, we infected *Irf5*^{-/-}, *Irf3*^{-/-} *Irf7*^{-/-}
108 DKO, or *Irf3*^{-/-} *Irf5*^{-/-} *Irf7*^{-/-} triple knockout (TKO) mice with OROV. Whereas the combined loss
109 of *Irf3* and *Irf7* or *Irf3*, *Irf5*, and *Irf7* expression resulted in rapid systemic disease with high
110 lethality rates and extensive virus replication in the liver, the deletion of *Irf5* alone yielded a
111 distinct phenotype. OROV infection in *Irf5*^{-/-} mice was associated with a protracted disease
112 that recapitulated features of human infection, with signs of neurological involvement and
113 high levels of virus accumulating in the brain and spinal cord.

114 **MATERIALS AND METHODS**

115 **Ethics statement.** This study was carried out in accordance with the
116 recommendations in the Guide for the Care and Use of Laboratory Animals of the National
117 Institutes of Health. The protocols were approved by the Institutional Animal Care and Use
118 Committee at the Washington University School of Medicine (Assurance Number: A3381-
119 01). Inoculations were performed under anesthesia that was induced and maintained with
120 ketamine hydrochloride and xylazine, and all efforts were made to minimize animal suffering.

121 **Viruses.** OROV (strain BeAn 19991) and LACV (original strain) were provided by E.
122 Arruda (São Paulo University, Ribeirão Preto, Brazil) and A. Pekosz (Johns Hopkins
123 University, Baltimore, Maryland, USA), respectively. OROV and LACV stocks were produced
124 in Vero cells. Studies with OROV were conducted under enhanced BSL-3 and A-BSL3
125 (Animal BSL-3) containment at Washington University School of Medicine with appropriate
126 personal protective equipment (respirators) and approval from the United States Department
127 of Agriculture. Experiments with LACV were performed under BSL-2 and A-BSL2 conditions.

128 **Mouse experiments.** WT C57BL/6 mice were purchased from Jackson
129 Laboratories. Congenic *Irfnar^{-/-}*, *Irf5^{-/-}*, *Irf3^{-/-} Irf7^{-/-}* DKO, and *Irf3^{-/-} Irf5^{-/-} Irf7^{-/-}* TKO mice have
130 been described previously (4, 18, 26, 27). *Irf5^{-/-}* mice were the gift of T. Taniguchi (Tokyo,
131 Japan), obtained from I. Rifkin (Boston, MA), and had been backcrossed for eight
132 generations. After detection of a homozygous *Dock2* mutation in this line, we backcrossed
133 *Irf5^{-/-}* mice for five additional generations and selected animals that were *Dock2^{wt/wt}* using
134 PCR-based genotyping (11). All mice were bred in a specific pathogen-free facility at
135 Washington University. Subcutaneous inoculations were performed by injection in the
136 footpad with 10⁶ FFU of OROV and 10⁵ FFU of LACV in a volume of 50 μ l. Intracranial
137 injections were performed with 10² FFU of OROV in a volume of 10 μ l. Infection experiments
138 were designed with 5 to 6 and 8 week-old mice for OROV and LACV, respectively. The 8
139 week-old mice were used with LACV because younger mice had a higher mortality rate in
140 WT mice, which limited our ability to detect differences in the KO mice. Survival and weight
141 loss monitored for 21 days.

142 **Measurement of viral burden.** OROV-infected mice were euthanized at days 4, 6, 9
143 and 12 post-infection. LACV-infected mice were euthanized at days 4, 8 and 12 post-
144 infection. Animals were perfused extensively with 20 ml of PBS at the time of euthanasia.
145 Liver, spleen, kidney, lung, heart, brain and spinal cord were harvested, weighed and
146 homogenized with zirconia beads in MagNA Lyser instrument (Roche Life Science) in 1 ml
147 of Minimal Essential Medium (MEM) supplemented with 2% heat-inactivated fetal bovine
148 serum (FBS). All homogenized tissues and approximately 200 μ l of serum from infected
149 animals were stored at -80°C until virus titration.

150 Viral burden was determined by focus-forming assay on Vero cells. Samples were
151 thawed, clarified by centrifugation (2,000 \times g at 4°C for 10 min), and then diluted serially
152 prior to infection of Vero cells in 96-well plates. Infected cell foci were detected 22 to 24 h
153 later, following overnight fixation with 1% paraformaldehyde and incubation with a 1:1,000
154 dilution of polyclonal mouse anti-OROV ascites fluid (ATCC, VR1228AF) or a 1:100 dilution
155 of hybridoma cell supernatants containing the anti-LACV monoclonal antibodies (MAbs) 807-
156 31 and 807-33 (provided by A. Pekosz), all in a volume of 50 μ l for 2 h at room temperature.
157 After incubation for 1 h with 50 μ l of a 1:2,000 dilution of horseradish peroxidase (HRP)-
158 conjugated goat anti-mouse IgG (Sigma), foci were detected by addition of TrueBlue
159 detection reagent (KPL). The spots were analyzed with a CTL Immunospot instrument.

160 **Measurement of viral RNA.** Tissue samples from WT and *Irf5*^{-/-} mice were extracted
161 with the RNeasy kit (Qiagen). OROV RNA levels in serum, liver, spleen, lung, kidney, brain
162 and spinal cord were determined by Taqman one-step qRT-PCR and expressed on a log₁₀
163 scale as viral RNA equivalents per gram or per ml after comparison with a standard curve
164 produced using serial ten-fold dilutions of OROV RNA. The amplification of *Gapdh* (IdT cat
165 no: Mm.PT.39a.1) was used as a control for normalization. All reactions were performed
166 using 300 ng of RNA, 2.5 μ l of 10X PrimeTime solution (IdT, OROV-F: 5'-
167 TACCCAGATGCGATCACCAA-3'; OROV-R: 5'- TTGCGTCACCATCATTCCAA -3'; OROV-
168 Probe: 5'-/56-FAM/ TGCCTTTGGCTGAGGTAAAGGGCTG/36-TAMSp/-3'), 12.5 μ l of

169 TaqMan master mix (Applied Biosystems) and 0.625 μ l of reverse transcriptase (Applied
170 Biosystems) in a final volume of 25 μ l. The cycling algorithm was: 48°C for 30 min, 95°C for
171 10 min and 45 cycles of 95°C for 15 s and 60°C for 1 min.

172 **Blood chemistry analysis.** Serum from WT, *Irf5*^{-/-}, or TKO mice was isolated on
173 days 4, 6, 9 and 12 after OROV infection. Chemistry analyses were performed using a
174 Catalyst Dx Chemistry Analyzer (IDEX Laboratories) after treatment with β -propiolactone
175 (BPL, Sigma) for 30 min at 37°C to inactivate infectious virus. Treatment with BPL did not
176 impact chemistry results.

177 **Cytokine bioplex assay.** At days 4, 6, 9 and 12 after OROV infection of WT, *Irf5*^{-/-},
178 and TKO mice, serum was collected and cytokine levels were measured using the Bioplex
179 Pro Mouse Cytokine Assay (BioRad). The levels of the following cytokines and chemokines
180 were determined: IL-1 α , IL-1 β , IL-2, IL-3, IL-4, IL-6, IL-9, IL-10, IL-12p40, IL-12p70, IL-13, IL-
181 17, Eotaxin (CCL11), G-CSF, GM-CSF, IFN- γ , KC (CXCL1), MCP-1 (CCL-2), MIP-1 α
182 (CCL3), MIP-1 β (CCL4), RANTES (CCL5) and TNF- α .

183 **Quantification of type I IFN activity.** Levels of type I IFN in the serum of WT and
184 *Irf5*^{-/-} mice at 1, 2, or 3 days after OROV were determined by an encephalomyocarditis virus
185 cytopathic effect bioassay in L929 cells as described previously (28). Briefly, all samples
186 were treated with citrate buffer (40 mM citric acid, 10 mM KCl, 135 mM NaCl [pH 3.0]) for 10
187 minutes and neutralized with Minimal Essential Medium buffered with 45 mM HEPES pH
188 8.0. The amount of type I IFN per ml of serum was calculated and compared to a standard
189 curve using recombinant IFN- α (PBL Assay Science).

190 **Histology, TUNEL staining, and immunohistochemistry.** Liver and spleen tissues
191 were obtained from WT, *Irf5*^{-/-}, and TKO mice at day 4 after OROV infection. Brain tissue
192 from WT and *Irf5*^{-/-} KO mice was harvested at day 12 after virus inoculation. All samples
193 were fixed in 4% paraformaldehyde (in PBS) for 24 h at 4°C, dehydrated in increasing
194 ethanol concentrations and embedded in paraffin. Hematoxylin/eosin staining of paraffin-
195 embedded tissues was performed by the Digestive Diseases Research Core Center
196 Morphology Core of the Washington University. Tdt-mediated dUTP nick end labeling

197 (TUNEL) staining from liver and spleen sections was performed using an *In Situ* Cell Death
198 Detection Kit POD (Roche) as described by the manufacturer. TUNEL staining of brain
199 sections was performed after permeabilization with proteinase K (Roche) for 30 minutes
200 using the Cell Death Detection KIT, TMR Red (Roche), followed by counter-staining with
201 DAPI (Invitrogen) for five minutes. As a positive control, tissue sections were treated with
202 DNase (Sigma) for 10 minutes to introduce nicks into DNA. Slides were visualized using an
203 Axioscope (Zeiss) microscope and images were captured using AxioCam HRm (Zeiss) and
204 Axiovision Rel4.8 (Zeiss) software.

205 For OROV antigen detection, tissues sections were deparaffinized, rehydrated, and
206 treated with citrate buffer (pH 6.0) for antigen retrieval. Endogenous peroxidases were
207 quenched by incubation with 4% H₂O₂ for 30 min and the antigen detection was performed
208 using the "Mouse on Mouse" (M.O.M.) immunodetection kit according to the manufacturer's
209 protocol (Vector Laboratories). All sections were incubated with an avidin/biotin blocking
210 solution and M.O.M. mouse immunoglobulin-blocking reagent for 15 min at room
211 temperature and then incubated with mouse polyclonal anti-OROV ascetic fluid (1:100) for 2
212 h at room temperature. Sections were then incubated with a M.O.M. biotinylated anti-mouse
213 IgG antibody for 1 hour and with a streptavidin-peroxidase Ultrasensitive Polymer (Sigma) for
214 15 min at room temperature. Antigen-positive cells were visualized at 20x and 40X
215 magnification in a Zeiss Axioskop microscope, and images were captured using a AxioCam
216 MRC digital color camera after incubation with DAB (3, 3'-diaminobenzidine) HRP substrate
217 (Vector) and counter-staining with hematoxylin.

218 **OROV replication in primary cells.** Macrophage (M ϕ) and DC cultures were
219 derived from bone marrow isolated from WT, *Irf5*^{-/-}, and TKO mice and cultured for seven
220 days in medium supplemented with 40 ng/ml M-CSF (PeproTech) or 20 ng/ml of both GM-
221 CSF and IL-4 (PeproTech), respectively. Multi-step virus growth curves were performed
222 using a multiplicity of infection (MOI) of 0.001. The viral titer in the cell-free supernatant was
223 determined by FFU assay on Vero cells at the following time points after infection: 0, 1, 4,
224 12, 24, 36, 48, and 60 h.

225 **Isolation of OROV-Infected cells.** Whole blood was collected in tubes containing
226 EDTA. Erythrocytes were removed after 10 min of incubation in Red Blood Cell Lysis
227 Solution Buffer (Miltenyi Biotech). Non-specific antibody binding was inhibited after
228 incubation with Fc block (BD Bioscience) for 15 min. Cell suspensions from six different WT
229 and *Irf5*^{-/-} mice were purified sequentially by positive selection with CD19, CD3 and CD11b
230 microbeads (Miltenyi Biotech), following the manufacturer's protocol. A separate experiment
231 was conducted to purify pDCs using B220 or CD11c microbeads (Miltenyi Biotech). All cell
232 populations were tested by qRT-PCR for OROV and *Gapdh* RNA levels and in parallel
233 analyzed by flow cytometry by staining with antibodies to CD3, CD19, CD11b, and CD11c.

234 **Quantification of *Iffa* and *Iffb* RNA.** The levels of *Iffa* and *Iffb* mRNA were
235 determined by qRT-PCR in DCs, M ϕ , and sorted cells from WT and *Irf5*^{-/-} mice, following
236 previously published procedures (25). Briefly, RNA from target cells was extracted using the
237 RNeasy kit (Qiagen) and treated with TURBO DNase (Life Technologies) for 2 h at 37°C.
238 qRT-PCR was performed by one-step reaction with previously indicated primers and probes
239 (25). All reactions were assembled in a final volume of 25 μ l with 300 ng of RNA, 1X
240 PrimeTime mix (Integrated DNA Technologies) and 12.5 μ l of TaqMan master mix (Applied
241 Biosystems) by using the previously indicated cycling algorithm. All reactions were
242 normalized to *Gapdh* RNA using primers and probe previously published (25) and expressed
243 on a log₂ scale as fold increase over mock according to the threshold cycle ($\Delta\Delta$ CT) method
244 (29).

245 **Quantitation of antibodies.** The titer of neutralizing antibodies was determined on
246 serum obtained at day 7 after OROV infection of WT and *Irf5*^{-/-} mice by a standard plaque
247 reduction neutralization assay (30). Plaques were scored visually after incubation with serial
248 dilutions of the mice serum and the 50% neutralization titer (PRNT₅₀) was determined.

249 **Data analysis.** All data were analyzed with Prism software (GraphPad Software).
250 Kaplan-Meier survival curves were analyzed by the log rank test and weight loss curve was
251 compared using 2-way ANOVA. For viral burden analysis, the log titers were analyzed by

252 the Mann-Whitney test. qRT-PCR results also were compared using 2-way ANOVA. A *P*
253 value of < 0.05 indicated statistically significant differences.

254

255

256 **RESULTS**

257 ***Irf3^{-/-} Irf5^{-/-} Irf7^{-/-} TKO mice are highly vulnerable to OROV infection.*** Because the
258 lethality in *Irf3^{-/-} Irf7^{-/-}* DKO mice after OROV infection was not as rapid nor complete as
259 observed in *Ifnar^{-/-}* mice (25) (**Fig 1A, C, and E**), we hypothesized that other transcription
260 factors implicated in the induction of antiviral immunity restricted OROV pathogenesis.
261 Accordingly, we evaluated OROV pathogenesis in 5 to 6 week-old *Irf3^{-/-} Irf5^{-/-} Irf7^{-/-}* TKO mice
262 after injection with 10⁶ FFU of OROV by a subcutaneous route. Analogous to results with
263 *Ifnar^{-/-}* mice, OROV infection of TKO mice caused rapid weight loss and resulted in 100%
264 mortality, with a mean of survival time of 4 days (**Fig 1A, C, and F**). OROV-infected *Irf3^{-/-}*
265 *Irf5^{-/-} Irf7^{-/-}* TKO mice exhibited lethargy and decreased body temperature, especially at day
266 4 after infection, but did not show signs of neuroinvasive disease, such as ataxia, seizures,
267 tremors, or paralysis.

268 **Vulnerability of *Irf5^{-/-}* mice to OROV infection.** To assess the role of IRF-5 in
269 restricting OROV infection more directly, we inoculated 5 to 6 week-old *Irf5^{-/-}* and congenic
270 wild-type (WT) mice with OROV. Whereas 39% of *Irf5^{-/-}* mice succumbed to OROV infection,
271 WT mice had no mortality or signs of morbidity (**Fig 1A and B**). *Irf5^{-/-}* mice exhibited a
272 protracted course of OROV disease compared to *Irf3^{-/-} Irf5^{-/-} Irf7^{-/-}* TKO mice with signs of
273 neurological involvement and lethality starting at days 7 and 9 after infection, respectively
274 (**Fig 1A, D, and F**). Almost 50% of *Irf5^{-/-}* OROV-infected mice developed signs of severe
275 disease after day 7, including lethargy, shivering, ataxia, limb paralysis, dyskinesia,
276 hypothermia, and weight loss.

277 **Viral burden studies.** To determine the basis for their susceptibility to OROV
278 infection, we inoculated WT, *Irf5^{-/-}*, *Irf3^{-/-} Irf7^{-/-}* DKO, and *Irf3^{-/-} Irf5^{-/-} Irf7^{-/-}* TKO mice and
279 measured viral burden in the serum, liver, spleen, kidney, lung, heart, brain and spinal cord
280 at days 4, 6, 9 and 12 after infection. As reported previously, infectious OROV was not
281 recovered from any site in WT mice at any of the days analyzed (25). In comparison, all *Irf3^{-/-}*
282 *Irf5^{-/-} Irf7^{-/-}* TKO mice developed viremia (3.4 x 10³ to 1.3 x 10⁸ FFU/ml), and infectious
283 OROV was recovered from the liver (4.2 x 10⁶ to 1.3 x 10⁹ FFU/g) and spleen (5.2 x 10⁶ to

284 1.9×10^{10} FFU/g) at day 4 after infection (**Fig 2A-C**). Infectious OROV also was present in
285 the kidneys (5.2×10^3 to 5.9×10^7 FFU/g) and lungs (1.3×10^3 to 4.8×10^7 FFU/g) of
286 approximately 50% of *Irf3*^{-/-} *Irf5*^{-/-} *Irf7*^{-/-} TKO mice on day 4 (**Fig 2D and E**). However, OROV
287 was not recovered from heart, brain, or spinal cord of *Irf3*^{-/-} *Irf5*^{-/-} *Irf7*^{-/-} TKO mice at this time
288 point (**Fig 2F-H**). The levels of OROV in the serum, liver and spleen of *Irf3*^{-/-} *Irf5*^{-/-} *Irf7*^{-/-} TKO
289 mice were similar to those reported for *Ifnar1*^{-/-} mice (post-hoc comparison with *Ifnar1*^{-/-} mice
290 (25): $P = 0.38$, 0.16 , and 0.14 , respectively) but greater those observed in *Irf3*^{-/-} *Irf7*^{-/-} DKO
291 mice ($P = 0.005$, 0.013 , and 0.003 , respectively).

292 In contrast to *Irf3*^{-/-} *Irf5*^{-/-} *Irf7*^{-/-} TKO mice, infectious OROV was detected only in the
293 brain and spinal cord at 9 days or after in *Irf5*^{-/-} mice (**Fig 2G and H**), and not in any of the
294 peripheral organs. At day 12, 9 of 13 (69%) *Irf5*^{-/-} mice had measurable OROV in the brain or
295 spinal cord, with high titers recovered (5.1×10^4 to 4.8×10^7 FFU/g and 5×10^5 to 8×10^7
296 FFU/g, respectively). In comparison, only 1 of 11 *Irf3*^{-/-} *Irf7*^{-/-} DKO mice had measurable
297 infectious OROV in the brain and spinal cord at days 9 after inoculation, and no virus was
298 measured at day 12 (**Fig 2G and H**). These results suggest that IRF-5, rather than IRF-3 or
299 IRF-7, preferentially regulates a stage of OROV control, which is essential for restricting
300 dissemination to or infection within the CNS.

301 To evaluate further whether IRF-5 limits OROV earlier in the course of infection, we
302 evaluated the viral burden levels by a more sensitive quantitative reverse transcriptase PCR
303 (qRT-PCR) assay. At day 6 after infection, higher levels of OROV RNA were observed in the
304 serum (188-fold, $P = 0.0001$), liver (248-fold, $P = 0.02$), spleen (55-fold, $P = 0.03$) and
305 kidneys (204-fold, $P = 0.0001$) of *Irf5*^{-/-} than WT mice (**Fig 2I-O**).

306 **Blood chemistry analysis reveals transient liver damage in OROV-infected *Irf5*^{-/-}**
307 **mice.** Our prior study showed that deficiencies of type I IFN signaling (*Ifnar1*^{-/-}), RIG-I-like
308 receptor signaling (*Mavs*^{-/-}), or downstream transcription factors (*Irf3*^{-/-} and *Irf7*^{-/-}) resulted in
309 uncontrolled replication of OROV in peripheral organs that was associated with extensive
310 liver damage (25). To assess whether visceral organ damage occurred in *Irf5*^{-/-} mice after
311 OROV infection, we measured the levels of alanine aminotransferase (ALT), aspartate

312 aminotransferase (AST), glucose (GLU), blood urea nitrogen (BUN), creatinine (CRE),
313 alkaline phosphatase (ALKP) and creatine kinase (CK) in the serum of WT, *Irf5*^{-/-}, and *Irf3*^{-/-}
314 *Irf5*^{-/-} *Irf7*^{-/-} TKO mice. Although BUN, ALKP, and CK levels were similar between infected
315 WT and KO animals (**Table 1**), higher levels of ALT (1,243 U/l and 969 U/l) and AST (1,097
316 U/l and 965U/l) and lower levels of GLU (262 mg/dl and 106 mg/dl) were detected in the
317 serum of *Irf3*^{-/-} *Irf5*^{-/-} *Irf7*^{-/-} TKO and *Irf5*^{-/-} mice at days 4 and 6 after OROV infection,
318 respectively compared to that observed in WT animals (**Fig 3A-C**). In contrast to that
319 observed in *Irf3*^{-/-} *Irf5*^{-/-} *Irf7*^{-/-} TKO and *Ifnar*^{-/-} mice (25), the lethality observed in *Irf5*^{-/-} mice
320 was not associated with massive hepatic injury, since the levels of ALT, AST and GLU
321 normalized at later time points, even in the subset of animals that became ill.

322 **Analysis of serum cytokine levels in *Irf5*^{-/-} mice infected with OROV.** IRF-5 has
323 been reported to regulate serum cytokine accumulation in the context of arthropod-borne
324 virus infections *in vivo* (11). We measured the levels of 23 cytokines and chemokines in
325 serum from WT, *Irf5*^{-/-}, and *Irf3*^{-/-} *Irf5*^{-/-} *Irf7*^{-/-} TKO mice on days 4, 6, 9 and 12 after OROV
326 infection. Similar to published data (25) in *Ifnar*^{-/-} and *Irf3*^{-/-} *Irf7*^{-/-} DKO mice, we did not
327 observe elevated levels of vasoactive (e.g., TNF- α) or inflammasome-generated (e.g., IL-1 β)
328 cytokines in the OROV-infected *Irf3*^{-/-} *Irf5*^{-/-} *Irf7*^{-/-} TKO or *Irf5*^{-/-} mice (**Table 2**). However, the
329 levels of other proinflammatory cytokines and chemokine were increased at day 4 after
330 OROV infection in *Irf3*^{-/-} *Irf5*^{-/-} *Irf7*^{-/-} TKO mice (e.g. IL-6, IL-12p40, G-CSF, KC and MIP-1 α ,
331 **Fig 4A-E**). Because the levels of all analyzed cytokines were similar between *Irf5*^{-/-} and WT
332 mice after OROV infection, the mild liver damage observed in *Irf5*^{-/-} mice is unlikely to be due
333 to a generalized cytokine storm.

334 To assess whether a deficiency of IRF-5 affected systemic type I IFN responses, we
335 measured type I IFN antiviral activity in serum from WT and *Irf5*^{-/-} animals at days 1, 2, and 3
336 after OROV infection using an established bioassay (28). At day 1 after OROV infection, *Irf5*^{-/-}
337 ^{-/-} and WT mice both had slightly higher levels of type I IFN than mock-infected mice (**Fig 4F**).
338 Type I IFN activity in serum waned in WT animals after 2 days of infection. However,
339 significant increases in type I IFN were apparent (~44-fold, *P* < 0.0001) at day 3 after OROV

340 injection in *Irf5*^{-/-} mice. These high levels of type I IFN in *Irf5*^{-/-} mice suggest an ongoing
341 OROV infection and a relatively intact systemic IFN response.

342 **OROV-induced disease in *Irf3*^{-/-} *Irf5*^{-/-} *Irf7*^{-/-} TKO mice is associated with viral**
343 **replication and hepatocyte death.** To characterize the basis of the liver injury observed in
344 *Irf3*^{-/-} *Irf5*^{-/-} *Irf7*^{-/-} TKO infected mice, we performed pathological analysis on hepatic tissue
345 isolated from WT, *Irf5*^{-/-}, and *Irf3*^{-/-} *Irf5*^{-/-} *Irf7*^{-/-} TKO mice at day 4 after OROV infection. While
346 hematoxylin and eosin staining revealed areas of edema and focal cellular necrosis in liver
347 sections of *Irf3*^{-/-} *Irf5*^{-/-} *Irf7*^{-/-} TKO mice, these changes were not apparent in samples from
348 WT and *Irf5*^{-/-} infected mice (**Fig 5A**). The liver damage in *Irf3*^{-/-} *Irf5*^{-/-} *Irf7*^{-/-} TKO mice was
349 associated with greater numbers of Tdt-mediated dUTP nick end labeling (TUNEL)-positive
350 (**Fig 5B**) and OROV antigen-positive hepatocytes (**Fig 5C**) at day 4 after infection. In
351 comparison, a smaller number of TUNEL and OROV positive cells were observed in the
352 livers of *Irf5*^{-/-} mice, and none were detected in WT mice.

353 **The effect IRF-5 on OROV-induced neuropathology.** Given the presence of
354 OROV in the brain and spinal cord of some *Irf5*^{-/-} mice (see **Fig 2**), we performed histological
355 analysis on brain sections from WT and *Irf5*^{-/-} mice to define why some animals succumbed
356 to infection. TUNEL-positive cells were detected in different regions of the brain, including
357 the cerebral cortex, hippocampus, midbrain, and cerebellum from OROV-infected *Irf5*^{-/-} mice
358 (**Fig 6A-D**). Moreover, abundant staining for viral antigen was detected in several regions of
359 the brain of OROV-infected *Irf5*^{-/-} mice but not in infected WT or uninfected *Irf5*^{-/-} mice (**Fig**
360 **7A-D**). In agreement with a published study that reported co-staining for viral antigen with a
361 neuron marker (NeuN) in newborn mice infected with OROV (31), the morphology of viral
362 antigen-positive cells in *Irf5*^{-/-} mice was consistent with neurons being targeted for infection
363 (**Fig 7B and C**), particularly in the hippocampus.

364 **WT and *Irf5*^{-/-} mice are equally vulnerable to OROV infection when inoculated**
365 **by an intracranial route.** To define whether the enhanced replication of OROV in the brains
366 of *Irf5*^{-/-} mice was due to an intrinsic inhibitory effect of IRF-5 in the CNS, we infected WT
367 and *Irf5*^{-/-} mice with OROV by an intracranial route and monitored morbidity, mortality, and

368 viral burden. We observed no differences in survival rates, weight loss, and viral load in the
369 brain WT and *Irf5*^{-/-} mice after intracranial infection (data not shown); 100% of WT and *Irf5*^{-/-}
370 mice succumbed to infection by day 7 after intracranial inoculation with no difference in
371 mean time to death (data not shown). These results suggest that IRF-5 does not have a
372 direct antiviral effect against OROV within the brain but rather is likely important for
373 restricting spread to the brain.

374 **OROV RNA persists in cells from *Irf5*^{-/-} mice.** To begin to define why a deficiency
375 of IRF-5 resulted in disseminated OROV infection in the CNS at such a relatively late time
376 point, we tested tissue samples for virus by qRT-PCR at days 9 and 12 after infection, which
377 immediately precedes the onset of lethality in *Irf5*^{-/-} mice (see **Fig 1**). Although samples from
378 all WT mice tested were negative for OROV RNA at day 12, indicating successful clearance,
379 the serum, liver, spleen, kidney, lung, brain, and spinal cord from more than 50% of *Irf5*^{-/-}
380 mice were positive for OROV RNA at this late time point (**Fig 8A-G**). Analogously, at day 9
381 after infection, 3 of 8 (37.5%) and 5 of 8 (62.5%) spinal cord and brain samples,
382 respectively, from *Irf5*^{-/-} mice were positive for OROV RNA, whereas none were positive in
383 infected WT mice (**Fig 8F and G**). The persistence of OROV in different peripheral organs in
384 *Irf5*^{-/-} mice could lead to the selection of an encephalitic variant of OROV with greater
385 neuroinvasive potential, as seen with the JC polyomavirus (32, 33). To test this idea, we
386 homogenized brain tissue from OROV-infected *Irf5*^{-/-} mice and used this to infect WT and
387 *Irf5*^{-/-} mice. These isolates were not more virulent or neuroinvasive than the parental OROV
388 used in this study in either WT or *Irf5*^{-/-} mice (data not shown).

389 As an alternative hypothesis, we speculated that persistently infected *Irf5*^{-/-} cells
390 might deliver OROV into the CNS. To determine which cells in *Irf5*^{-/-} mice harbored OROV
391 RNA during late stages of this disease, WT and *Irf5*^{-/-} mice were infected with OROV. As we
392 did not have a fluorescence activated cell sorter in our enhanced BSL3 suite, at day 8 after
393 viral infection, different cell populations were purified from blood by positive selection with
394 anti-CD19, -CD3, -CD11b, -B220 or -CD11c magnetic beads (**Fig 9A-B**) and tested by qRT-
395 PCR for the presence of OROV RNA. Populations of CD11c⁺ and B220⁺ cells from *Irf5*^{-/-}

396 mice were frequently (~50%) positive for OROV (**Fig 9C**) suggesting these cells might
397 transport virus into the brain directly or propagate virus sufficiently to allow crossing of the
398 blood-brain barrier (BBB) in the fluid phase.

399 To evaluate whether a deficiency of IRF-5 could affect the expression of type I IFN in
400 DCs *in vivo*, we measured the levels of *Ifnb* mRNA in CD11c⁺, B220⁺, CD11c⁻ and B220⁻ cell
401 populations from WT and *Irf5*^{-/-} mice obtained 8 days after OROV infection. The levels of *Ifnb*
402 mRNA were lower in circulating cells ((including CD11c⁺ (18-fold, *P* < 0.05) and B220⁺ cells
403 (23-fold, *P* < 0.05)) from *Irf5*^{-/-} infected mice in comparison to WT mice (**Fig 9D**) despite the
404 increased levels of OROV infection. This data suggests that IRF-5 signaling is essential to
405 induce optimal type I IFN responses in peripheral blood mononuclear cells after OROV
406 infection.

407 **OROV replication is enhanced and the production of type I IFN is diminished in**
408 **DCs from *Irf5*^{-/-} mice.** As DCs from *Irf5*^{-/-} mice produced less *Ifnb* and appeared to support
409 greater OROV replication in blood, to corroborate these findings, we evaluated viral growth
410 kinetics and type I IFN mRNA expression in bone marrow-derived DCs and M ϕ from WT,
411 *Irf5*^{-/-}, and *Irf3*^{-/-} *Irf5*^{-/-} *Irf7*^{-/-} TKO mice. In DCs, OROV infection was greater in cells derived
412 from *Irf3*^{-/-} *Irf5*^{-/-} *Irf7*^{-/-} TKO cells (> 10,000-fold (*P* < 0.01)) at 36 to 60 hours compared to WT
413 cells, which failed to support productive infection (**Fig 10A**). Higher levels (130 to 1,750-fold
414 higher, *P* < 0.05) of viral replication also were observed in DCs from *Irf5*^{-/-} compared to WT
415 mice. In comparison, in M ϕ , productive OROV infection was detected only in cells derived
416 from *Irf3*^{-/-} *Irf5*^{-/-} *Irf7*^{-/-} TKO and not WT or *Irf5*^{-/-} mice (**Fig 10B**). Thus, in cell culture a
417 deficiency of IRF5 resulted in enhanced OROV infection specifically in DCs, which supports
418 our *ex vivo* and *in vivo* findings of elevated OROV RNA in *Irf5*^{-/-} CD11c⁺ cells and sustained
419 viremia and spread to the CNS in *Irf5*^{-/-} mice. Moreover, and despite the higher levels of
420 OROV infection, lower levels *Ifna* and *Ifnb* mRNA were observed in bone marrow-derived
421 DCs from *Irf5*^{-/-} compared to WT mice (**Fig 10C and D**). A lesser impact of IRF-5 on *Ifna* but

422 not *lfnb* mRNA induction was observed in bone marrow-derived M ϕ after OROV infection
423 (Fig 10E and F).

424 **Effect of IRF-5 on antibody responses after OROV infection.** WT mice efficiently
425 cleared OROV infection from all tissue compartments whereas infection persisted in mice
426 lacking IRF-5. Given prior studies demonstrating skewed antibody isotype responses,
427 deficient B cell maturation, and low levels of antigen-specific memory B cells in *Irf5*^{-/-} mice (9,
428 11, 34), we hypothesized that IRF-5 might be required for optimal adaptive immunity against
429 OROV. To evaluate the role of IRF-5 in the humoral response against OROV, we
430 determined the titers of neutralizing antibody at day 7 and 12 after infection in WT and *Irf5*^{-/-}
431 mice (Figure 11A and B). *Irf5*^{-/-} mice had only slightly lower neutralizing titers at day 8 (2.1-
432 fold, $P < 0.005$) and 12 (1.5-fold, $P < 0.01$) than WT mice. To assess the importance of IRF-
433 5 on B cell response against OROV, we generated bone marrow chimeric mice that differed
434 only in the expression of IRF-5 in B cells. We adoptively transferred WT + μ MT (lacking all
435 mature B cells) or *Irf5*^{-/-} + μ MT bone marrow cells from CD45.2 mice into sublethally
436 irradiated 4-week-old WT CD45.1 recipient mice. Eight weeks later, the reconstitution of
437 donor immune cell populations in blood was confirmed by flow cytometry and all recipient
438 animals were infected with 10⁶ FFU of OROV (data not shown). However, no difference in
439 weight loss or viral load in the brain at day 12 was observed between the two groups (data
440 not shown). Thus, we did not observe a B cell-intrinsic role for IRF-5 in protection against
441 OROV infection in the CNS.

442 **IRF-5 restricts the neuropathogenesis of other orthobunyavirus.** To evaluate
443 whether IRF-5 also restricts infection of other orthobunyaviruses *in vivo*, we infected 8 week
444 old WT, *Irf5*^{-/-}, *Irf3*^{-/-} *Irf7*^{-/-} DKO, and *Irf3*^{-/-} *Irf5*^{-/-} *Irf7*^{-/-} TKO mice with LACV (10⁵ FFU), a
445 related encephalitic orthobunyavirus. Similar to our results with OROV, rapid lethality was
446 observed after LACV infection of *Irf3*^{-/-} *Irf7*^{-/-} DKO and *Irf3*^{-/-} *Irf5*^{-/-} *Irf7*^{-/-} TKO mice (Figure
447 12A). Remarkably, *Irf5*^{-/-} mice infected with LACV, failed to gain weight, showed clinical
448 signs of neuroinvasive disease and succumbed to infection after day 9 (Figure 12B-E).

449 Consistent with this, higher titers of LACV were observed in the brain and spinal cord (290 to
450 50,000-fold, $P < 0.05$) of *Irf5*^{-/-} mice at days 8 and 12 after infection compared to WT mice
451 (**Figure 12F-G**). These results establish that IRF-5 restricts infection and neuropathogenesis
452 of two different orthobunyaviruses.
453

454 **DISCUSSION**

455 Our study describes an innate immune mechanism for restricting neuroinvasion of
456 two different orthobunyaviruses that cause meningitis and encephalitis. IRF-5, a transcription
457 factor that is activated after recognition of pathogen-associated molecular patterns (4),
458 orchestrates a host response that controls bunyavirus neuroinvasion in infected mice. *Irf5*^{-/-}
459 mice died beginning at 12 days after OROV infection, a time when high levels of infectious
460 virus were detected exclusively in the brain and spinal cord. The relative importance of IRF-5
461 to the antiviral response against OROV is highlighted by comparisons with *Irf3*^{-/-} or *Irf7*^{-/-}
462 single KO mice, which sustained no or substantially lower levels of mortality after infection
463 (25). Moreover, significant levels of OROV infection were observed in the CNS of *Irf5*^{-/-} but
464 not in *Irf3*^{-/-} *Irf7*^{-/-} DKO mice. Thus, IRF-5, rather than IRF-3 and/or IRF-7, regulates a stage
465 in the control of OROV pathogenesis that prevents dissemination to the brain and spinal
466 cord.

467 Apart from its effect on neuroinvasion, IRF-5 also restricted OROV replication in the
468 liver, spleen and blood at earlier stages of infection. The evidence for this comes from
469 studies with *Irf5*^{-/-} mice and also by comparing OROV pathogenesis between *Irf3*^{-/-} *Irf7*^{-/-} DKO
470 and *Irf3*^{-/-} *Irf5*^{-/-} *Irf7*^{-/-} TKO mice. The *Irf3*^{-/-} *Irf5*^{-/-} *Irf7*^{-/-} TKO mice were highly vulnerable to
471 OROV infection and succumbed with similar kinetics compared to *Ifnar*^{-/-} mice (25), whereas
472 DKO mice were less susceptible. Accordingly, the levels of infectious virus in the liver,
473 spleen and blood were higher in *Irf3*^{-/-} *Irf5*^{-/-} *Irf7*^{-/-} TKO mice compared to *Irf3*^{-/-} *Irf7*^{-/-} DKO
474 mice (25). Consistent with a role for IRF-5 in restricting OROV replication in peripheral
475 organs, higher levels of viral RNA were detected in the serum, liver, spleen and kidneys of
476 *Irf5*^{-/-} compared to WT mice at day 6 after infection.

477 OROV infection of 5 to 6 week-old *Irf5*^{-/-} mice caused encephalitis after subcutaneous
478 inoculation. The morphology of the antigen-positive cells observed in the brain of *Irf5*^{-/-} mice
479 was consistent with neurons as a primary target of infection. Previously, OROV was reported
480 to cause encephalitis in newborn inbred WT mice, and was associated with paralysis and
481 mortality (31). OROV was recovered from the brain and spinal cord at days 4 and 5 days

482 after infection of newborns, and was detected almost exclusively in neurons (31). OROV
483 also induced meningoencephalitis in adult golden hamsters, with viral antigen present in
484 brain cells that morphologically resembled neurons (35). We also observed that ~40% of 8
485 week-old *Irf5*^{-/-} mice infected with LACV developed signs of neurological involvement,
486 including dyskinesia and paresis. In all symptomatic animals, we recovered infectious LACV.

487 How does IRF-5 control bunyavirus neuropathogenesis? We initially hypothesized
488 that IRF-5 could affect viral replication directly in neurons. However, and as seen with the
489 unrelated encephalitic flavivirus, WNV (11), no major differences in viral burden in the brain
490 were observed between WT and *Irf5*^{-/-} mice after intracranial inoculation of OROV. This
491 result suggests that the protective effect of IRF-5 against OROV or LACV is not due to a
492 CNS-intrinsic antiviral mechanism. Given these findings, we evaluated whether a deficiency
493 of IRF-5 affected OROV replication in circulating PBMCs, which could contribute to viremia
494 or possibly crossing of virus into the brain via a “Trojan horse” mechanism (36). Analysis of
495 viral RNA levels obtained from purified PBMC subsets of OROV-infected mice revealed that
496 B220⁺ and CD11c⁺ cell subsets from *Irf5*^{-/-} mice supported higher levels of OROV infection.
497 However, these OROV-expressing cells were not sufficient to infect the CNS, as adoptive
498 transfer of PBMCs or DCs from OROV-infected *Irf5*^{-/-} mice did not induce disease in naïve
499 WT or *Irf5*^{-/-} mice (data not shown). This result was not entirely unexpected since infection of
500 leukocytes alone does not disrupt the BBB in other viral models (37, 38). Although further
501 experiments are warranted, IRF-5 could regulate expression of molecules that sustain the
502 BBB integrity. An absence of IRF-5 then would result in increased viremia, infection of
503 PBMCs, and BBB permeability, all of which together could promote virus neuroinvasion.

504 Because both B220⁺ and CD11c⁺ purified cells were positive for OROV RNA at later
505 time points (day 8) after viral infection, we speculated that the plasmacytoid DC (pDC)
506 subset might be a primary target. IRF-5 regulates both IL-6 and IFN- β gene expression in
507 pDCs (12), and these cells are a primary source of type I IFNs and proinflammatory
508 cytokines after virus infection (17, 39). Although a definitive identification of pDCs as the key
509 DC subset regulating CNS infection of OROV and LACV in *Irf5*^{-/-} mice warrants further study,

510 we observed lower expression levels of *Irf5* mRNA after OROV infection in DCs *in*
511 *vivo* and in cell culture. Thus, infection of specific subsets of DCs, including possibly pDCs,
512 could modulate the production of antiviral cytokines and control of viral infection in blood. For
513 bunyaviruses, this process appears to require an optimal IRF-5 signaling pathway, as in its
514 absence viral persistence in serum occurs, and this is associated with neuroinvasion. This
515 process appears to be cell type-dependent, as in M ϕ an absence of IRF-5 did not impact
516 OROV infection or IFN- β induction, and we observed no decrease in overall type I IFN levels
517 in the serum of *Irf5*^{-/-} mice at days 1, 2, or 3 infection. Rather, type I IFN levels were higher in
518 the serum of *Irf5*^{-/-} mice at day 3 after infection; although the mechanism remains uncertain,
519 this phenotype could reflect greater levels of OROV replication in another cell type or tissue.

520 IRF-5 is essential to B cell differentiation and modulates the expression of the
521 plasma B cell maturation factor, Blimp-1 (9). *Irf5*^{-/-} mice have fewer T cells, B cells, NK cells,
522 M ϕ , and DCs in the draining lymph node at day 2 after WNV infection than WT mice, and
523 these mice have defects in generating an optimal acute and memory B cell response (11).
524 Although *Irf5*^{-/-} had slightly lower levels of neutralizing antibody against OROV at day 7 after
525 infection, it is unclear if these small differences contributed to neuroinvasion. Bone marrow
526 chimera reconstitution studies failed to show a protective role for IRF-5 in the B cell
527 compartment.

528 In summary, our study shows that IRF-5 is a key component of the immune response
529 against orthobunyaviruses, and contributes to restricting neuroinvasion. This phenotype was
530 associated with the defects in the control of replication and clearance of virus from
531 circulating PBMCs. The persistent circulation of virus in the blood of *Irf5*^{-/-} mice correlated
532 with neuroinvasion and viral burden in the brain and spinal cord. Future studies with
533 conditionally targeted IRF-5-deficient mice are planned to define the role of IRF-5 in specific
534 cell types on neuroinvasion. The animal model described here may be useful for
535 understanding the basic biology of the encephalitis induced by OROV, as well as testing
536 candidate therapeutics and vaccines. Finally, the antiviral activity of IRF-5 against different

537 families of viruses capable of causing lethal CNS infection could explain the selection and
538 perpetuation of gain-of-function *IRF5* alleles in the human population.

539

540 **ACKNOWLEDGMENTS**

541 The National Institutes of Health (R01 AI104972 and U19 AI083019 to M.S.D and
542 P30 DK52574 to Digestive Diseases Research Core Center Morphology Core), Conselho
543 Nacional de Desenvolvimento Científico e Tecnológico (CNPq)–Science Without Borders
544 (246513/2012-8 to J.L.P.-M), and a University Research Committee Award. We gratefully
545 acknowledge the technical assistance of Jennifer Govero, Michelle Noll, and Soila
546 Sukupolvi-Petty.

547

548

549 REFERENCES

- 550 1. **Taniguchi T, Ogasawara K, Takaoka A, Tanaka N.** 2001. IRF family of
551 transcription factors as regulators of host defense. *Annual review of immunology*
552 **19**:623-655.
- 553 2. **Paun A, Pitha PM.** 2007. The IRF family, revisited. *Biochimie* **89**:744-753.
- 554 3. **Akira S, Uematsu S, Takeuchi O.** 2006. Pathogen recognition and innate immunity.
555 *Cell* **124**:783-801.
- 556 4. **Takaoka A, Yanai H, Kondo S, Duncan G, Negishi H, Mizutani T, Kano S, Honda**
557 **K, Ohba Y, Mak TW, Taniguchi T.** 2005. Integral role of IRF-5 in the gene induction
558 programme activated by Toll-like receptors. *Nature* **434**:243-249.
- 559 5. **Izaguirre A, Barnes BJ, Amrute S, Yeow WS, Megjugorac N, Dai J, Feng D,**
560 **Chung E, Pitha PM, Fitzgerald-Bocarsly P.** 2003. Comparative analysis of IRF and
561 IFN-alpha expression in human plasmacytoid and monocyte-derived dendritic cells.
562 *Journal of leukocyte biology* **74**:1125-1138.
- 563 6. **Barnes BJ, Richards J, Mancl M, Hanash S, Beretta L, Pitha PM.** 2004. Global
564 and distinct targets of IRF-5 and IRF-7 during innate response to viral infection. *The*
565 *Journal of biological chemistry* **279**:45194-45207.
- 566 7. **Mori T, Anazawa Y, Iizumi M, Fukuda S, Nakamura Y, Arakawa H.** 2002.
567 Identification of the interferon regulatory factor 5 gene (IRF-5) as a direct target for
568 p53. *Oncogene* **21**:2914-2918.
- 569 8. **Barnes BJ, Kellum MJ, Pinder KE, Frisancho JA, Pitha PM.** 2003. Interferon
570 regulatory factor 5, a novel mediator of cell cycle arrest and cell death. *Cancer*
571 *research* **63**:6424-6431.
- 572 9. **Lien C, Fang CM, Huso D, Livak F, Lu R, Pitha PM.** 2010. Critical role of IRF-5 in
573 regulation of B-cell differentiation. *Proceedings of the National Academy of Sciences*
574 *of the United States of America* **107**:4664-4668.
- 575 10. **Panchanathan R, Liu H, Liu H, Fang CM, Erickson LD, Pitha PM, Choubey D.**
576 2012. Distinct regulation of murine lupus susceptibility genes by the IRF5/Blimp-1
577 axis. *J Immunol* **188**:270-278.
- 578 11. **Thackray LB, Shrestha B, Richner JM, Miner JJ, Pinto AK, Lazear HM, Gale M,**
579 **Jr., Diamond MS.** 2014. Interferon regulatory factor 5-dependent immune responses
580 in the draining lymph node protect against West Nile virus infection. *Journal of*
581 *virology* **88**:11007-11021.
- 582 12. **Steinhagen F, McFarland AP, Rodriguez LG, Tewary P, Jarret A, Savan R,**
583 **Klinman DM.** 2013. IRF-5 and NF-kappaB p50 co-regulate IFN-beta and IL-6
584 expression in TLR9-stimulated human plasmacytoid dendritic cells. *European journal*
585 *of immunology* **43**:1896-1906.
- 586 13. **Graham RR, Kozyrev SV, Baechler EC, Reddy MV, Plenge RM, Bauer JW,**
587 **Ortmann WA, Koeuth T, Gonzalez Escribano MF, Argentine, Spanish**
588 **Collaborative G, Pons-Estel B, Petri M, Daly M, Gregersen PK, Martin J,**
589 **Altshuler D, Behrens TW, Alarcon-Riquelme ME.** 2006. A common haplotype of
590 interferon regulatory factor 5 (IRF5) regulates splicing and expression and is
591 associated with increased risk of systemic lupus erythematosus. *Nature genetics*
592 **38**:550-555.
- 593 14. **Miceli-Richard C, Comets E, Loiseau P, Puechal X, Hachulla E, Mariette X.** 2007.
594 Association of an IRF5 gene functional polymorphism with Sjogren's syndrome.
595 *Arthritis and rheumatism* **56**:3989-3994.
- 596 15. **Kristjansdottir G, Sandling JK, Bonetti A, Roos IM, Milani L, Wang C,**
597 **Gustafsdottir SM, Sigurdsson S, Lundmark A, Tienari PJ, Koivisto K, Elovaara**
598 **I, Pirttila T, Reunanen M, Peltonen L, Saarela J, Hillert J, Olsson T, Landegren**
599 **U, Alcina A, Fernandez O, Leyva L, Guerrero M, Lucas M, Izquierdo G,**
600 **Matesanz F, Syvanen AC.** 2008. Interferon regulatory factor 5 (IRF5) gene variants
601 are associated with multiple sclerosis in three distinct populations. *Journal of medical*
602 *genetics* **45**:362-369.

- 603 16. **Dideberg V, Kristjansdottir G, Milani L, Libioulle C, Sigurdsson S, Louis E,**
604 **Wiman AC, Vermeire S, Rutgeerts P, Belaiche J, Franchimont D, Van Gossum**
605 **A, Bours V, Syvanen AC.** 2007. An insertion-deletion polymorphism in the interferon
606 regulatory Factor 5 (IRF5) gene confers risk of inflammatory bowel diseases. *Human*
607 *molecular genetics* **16**:3008-3016.
- 608 17. **Paun A, Reinert JT, Jiang Z, Medin C, Balkhi MY, Fitzgerald KA, Pitha PM.** 2008.
609 Functional characterization of murine interferon regulatory factor 5 (IRF-5) and its
610 role in the innate antiviral response. *The Journal of biological chemistry* **283**:14295-
611 14308.
- 612 18. **Lazear HM, Lancaster A, Wilkins C, Suthar MS, Huang A, Vick SC, Clepper L,**
613 **Thackray L, Brassil MM, Virgin HW, Nikolich-Zugich J, Moses AV, Gale M, Jr.,**
614 **Fruh K, Diamond MS.** 2013. IRF-3, IRF-5, and IRF-7 coordinately regulate the type I
615 IFN response in myeloid dendritic cells downstream of MAVS signaling. *PLoS*
616 *pathogens* **9**:e1003118.
- 617 19. **Vasconcelos HB, Nunes MR, Casseb LM, Carvalho VL, Pinto da Silva EV, Silva**
618 **M, Casseb SM, Vasconcelos PF.** 2011. Molecular epidemiology of Oropouche
619 virus, Brazil. *Emerging infectious diseases* **17**:800-806.
- 620 20. **Forshey BM, Guevara C, Laguna-Torres VA, Cespedes M, Vargas J, Gianella A,**
621 **Vallejo E, Madrid C, Aguayo N, Gotuzzo E, Suarez V, Morales AM, Beingolea L,**
622 **Reyes N, Perez J, Negrete M, Rocha C, Morrison AC, Russell KL, Blair PJ,**
623 **Olson JG, Kochel TJ, Group NFSW.** 2010. Arboviral etiologies of acute febrile
624 illnesses in Western South America, 2000-2007. *PLoS neglected tropical diseases*
625 **4**:e787.
- 626 21. **Watts DM, Lavera V, Callahan J, Rossi C, Oberste MS, Roehrig JT, Cropp CB,**
627 **Karabatsos N, Smith JF, Gubler DJ, Wooster MT, Nelson WM, Hayes CG.** 1997.
628 Venezuelan equine encephalitis and Oropouche virus infections among Peruvian
629 army troops in the Amazon region of Peru. *The American journal of tropical medicine*
630 *and hygiene* **56**:661-667.
- 631 22. **Bastos Mde S, Figueiredo LT, Naveca FG, Monte RL, Lessa N, Pinto de**
632 **Figueiredo RM, Gimaque JB, Pivoto Joao G, Ramasawmy R, Mourao MP.** 2012.
633 Identification of Oropouche Orthobunyavirus in the cerebrospinal fluid of three
634 patients in the Amazonas, Brazil. *The American journal of tropical medicine and*
635 *hygiene* **86**:732-735.
- 636 23. **Bastos MS, Lessa N, Naveca FG, Monte RL, Braga WS, Figueiredo LT,**
637 **Ramasawmy R, Mourao MP.** 2014. Detection of Herpesvirus, Enterovirus, and
638 Arbovirus infection in patients with suspected central nervous system viral infection in
639 the Western Brazilian Amazon. *Journal of medical virology* **86**:1522-1527.
- 640 24. **Pinheiro FP, Rocha AG, Freitas RB, Ohana BA, Travassos da Rosa AP, Rogerio**
641 **JS, Linhares AC.** 1982. [Meningitis associated with Oropouche virus infections].
642 *Revista do Instituto de Medicina Tropical de Sao Paulo* **24**:246-251.
- 643 25. **Proenca-Modena JL, Sesti-Costa R, Pinto AK, Richner JM, Lazear HM, Lucas T,**
644 **Hyde JL, Diamond MS.** 2015. Oropouche virus infection and pathogenesis is
645 restricted by MAVS, IRF-3, IRF-7, and type I IFN signaling pathways in non-myeloid
646 cells. *Journal of virology*.
- 647 26. **Daffis S, Suthar MS, Szretter KJ, Gale M, Jr., Diamond MS.** 2009. Induction of
648 IFN-beta and the innate antiviral response in myeloid cells occurs through an IPS-1-
649 dependent signal that does not require IRF-3 and IRF-7. *PLoS pathogens*
650 **5**:e1000607.
- 651 27. **Takaoka A, Mitani Y, Suemori H, Sato M, Yokochi T, Noguchi S, Tanaka N,**
652 **Taniguchi T.** 2000. Cross talk between interferon-gamma and -alpha/beta signaling
653 components in caveolar membrane domains. *Science* **288**:2357-2360.
- 654 28. **Thackray LB, Duan E, Lazear HM, Kambal A, Schreiber RD, Diamond MS, Virgin**
655 **HW.** 2012. Critical role for interferon regulatory factor 3 (IRF-3) and IRF-7 in type I
656 interferon-mediated control of murine norovirus replication. *Journal of virology*
657 **86**:13515-13523.

- 658 29. **Livak KJ, Schmittgen TD.** 2001. Analysis of relative gene expression data using
659 real-time quantitative PCR and the $2^{-(\Delta\Delta C(T))}$ Method. *Methods* **25**:402-
660 408.
- 661 30. **Diamond MS, Sitati EM, Friend LD, Higgs S, Shrestha B, Engle M.** 2003. A critical
662 role for induced IgM in the protection against West Nile virus infection. *The Journal of*
663 *experimental medicine* **198**:1853-1862.
- 664 31. **Santos RI, Almeida MF, Paula FE, Rodrigues AH, Saranzo AM, Paula AE, Silva**
665 **ML, Correa VM, Acrani GO, Neder L, Arruda E.** 2012. Experimental infection of
666 suckling mice by subcutaneous inoculation with Oropouche virus. *Virus research*
667 **170**:25-33.
- 668 32. **Ferenczy MW, Marshall LJ, Nelson CD, Atwood WJ, Nath A, Khalili K, Major EO.**
669 2012. Molecular biology, epidemiology, and pathogenesis of progressive multifocal
670 leukoencephalopathy, the JC virus-induced demyelinating disease of the human
671 brain. *Clinical microbiology reviews* **25**:471-506.
- 672 33. **Maginnis MS, Stroh LJ, Gee GV, O'Hara BA, Derdowski A, Stehle T, Atwood**
673 **WJ.** 2013. Progressive multifocal leukoencephalopathy-associated mutations in the
674 JC polyomavirus capsid disrupt lactoseries tetrasaccharide c binding. *mBio*
675 **4**:e00247-00213.
- 676 34. **Yasuda K, Nundel K, Watkins AA, Dhawan T, Bonegio RG, Ubellacker JM,**
677 **Marshak-Rothstein A, Rifkin IR.** 2013. Phenotype and function of B cells and
678 dendritic cells from interferon regulatory factor 5-deficient mice with and without a
679 mutation in DOCK2. *International immunology* **25**:295-306.
- 680 35. **Rodrigues AH, Santos RI, Arisi GM, Bernardes ES, Silva ML, Rossi MA, Lopes**
681 **MB, Arruda E.** 2011. Oropouche virus experimental infection in the golden hamster
682 (*Mesocricetus auratus*). *Virus research* **155**:35-41.
- 683 36. **Gras G, Kaul M.** 2010. Molecular mechanisms of neuroinvasion by monocytes-
684 macrophages in HIV-1 infection. *Retrovirology* **7**:30.
- 685 37. **Roe K, Kumar M, Lum S, Orillo B, Nerurkar VR, Verma S.** 2012. West Nile virus-
686 induced disruption of the blood-brain barrier in mice is characterized by the
687 degradation of the junctional complex proteins and increase in multiple matrix
688 metalloproteinases. *The Journal of general virology* **93**:1193-1203.
- 689 38. **Roe K, Orillo B, Verma S.** 2014. West Nile virus-induced cell adhesion molecules
690 on human brain microvascular endothelial cells regulate leukocyte adhesion and
691 modulate permeability of the in vitro blood-brain barrier model. *PloS one* **9**:e102598.
- 692 39. **Siegal FP, Kadowaki N, Shodell M, Fitzgerald-Bocarsly PA, Shah K, Ho S,**
693 **Antonenko S, Liu YJ.** 1999. The nature of the principal type 1 interferon-producing
694 cells in human blood. *Science* **284**:1835-1837.
- 695
- 696

697 **FIGURE LEGENDS**

698 **Figure 1. *Irf3*^{-/-} *Irf5*^{-/-} *Irf7*^{-/-} TKO mice are vulnerable to OROV infection, whereas**
699 **deletion of IRF-5 alone induces a disease with a protracted course. A.** Survival analysis
700 of 6 week-old mice after inoculation with 10⁶ PFU of OROV by subcutaneous inoculation in
701 the footpad: WT (n = 33), *Ifnar*^{-/-} (n = 25), *Irf5*^{-/-} (n = 33), *Irf3*^{-/-} *Irf7*^{-/-} DKO (n = 39), and *Irf3*^{-/-}
702 *Irf5*^{-/-} *Irf7*^{-/-} TKO (n = 17) mice were used. Data are pooled from at least three independent
703 experiments. Asterisks indicate differences that were statistically significant compared to WT
704 mice by the log rank test (****, *P* < 0.0001). **B-F.** Weight loss of infected (dead or surviving
705 animals considered separately) and non-infected WT (**B**) [n = 33 and n = 10 for infected and
706 non-infected mice, respectively), *Ifnar*^{-/-} (**C**) (n = 25 infected and n = 3 non-infected), *Irf5*^{-/-} (**D**)
707 (n = 20 dead, n = 13 survivors, and n = 4 non-infected), *Irf3*^{-/-} *Irf7*^{-/-} DKO (**E**) (n = 19 dead, n =
708 20 survivors, and n = 13 non-infected), and *Irf3*^{-/-} *Irf5*^{-/-} *Irf7*^{-/-} TKO (**F**) (n = 17 infected, n = 3
709 non-infected) mice. The weight loss curves were compared using 2-way ANOVA. Asterisks
710 indicate differences that were statistically significant compared to non-infected mice (*, *P* <
711 0.05; **, *P* < 0.01; ***, *P* < 0.001).

712 **Figure 2. Viral burden in mice infected with OROV. A-H.** Viral burden after OROV
713 infection of WT, *Irf5*^{-/-}, *Irf3*^{-/-} *Irf7*^{-/-} DKO and *Irf3*^{-/-} *Irf5*^{-/-} *Irf7*^{-/-} TKO mice was measured by
714 focus-forming assay in samples from serum (**A**), liver (**B**), spleen (**C**), kidney (**D**), lung (**E**),
715 heart (**F**), brain (**G**), and spinal cord (**H**). **I-O.** Viral burden after OROV infection of WT and
716 *Irf5*^{-/-} mice was determined by qRT-PCR in samples from serum (**I**), liver (**J**), spleen (**K**),
717 kidney (**L**), lung (**M**), brain (**N**), and spinal cord (**O**). Data points represent individual mice.
718 Bars indicate median values and were obtained from 6 to 15 mice per time point. Dashed
719 lines represent the limit of sensitivity of the assay. Asterisks indicate statistical significance
720 as judged by the Mann-Whitney test with a comparison to WT mice (*, *P* < 0.05; **, *P* < 0.01;
721 ***, *P* < 0.001, ****, *P* < 0.0001). A blue cross indicates that all OROV-infected TKO animals
722 were dead at the indicated time point. The viral burden data from *Irf3*^{-/-} *Irf7*^{-/-} DKO mice at
723 days 4 and 6 after OROV infection was published previously (25), and is provided as a
724 comparison to the *Irf3*^{-/-} *Irf5*^{-/-} *Irf7*^{-/-} TKO mice.

725 **Figure 3. Blood chemistry reveals liver injury after OROV infection in *Irf5*^{-/-} and**
726 ***Irf3*^{-/-} *Irf5*^{-/-} *Irf7*^{-/-} TKO mice. A-C.** Alanine aminotransferase (ALT, **A**), aspartate
727 aminotransferase (AST, **B**) and glucose (GLU, **C**) levels were measured from serum
728 samples of WT, *Irf5*^{-/-} and *Irf3*^{-/-} *Irf5*^{-/-} *Irf7*^{-/-} TKO mice (n= 4 to 13 for each group) obtained 4,
729 6, 9 and 12 days after infection with 10⁶ FFU of OROV. Data points represent individual mice
730 and were pooled from two independent experiments. Asterisks indicate statistical
731 significance compared to WT mice as judged by the Mann-Whitney test (*, *P* < 0.05; **, *P* <
732 0.01; ***, *P* < 0.001, ****, *P* < 0.0001). Dashed lines represent the mean values obtained
733 from three mock-infected animals.

734 **Figure 4. Serum cytokine levels in OROV-infected *Irf5*^{-/-} and *Irf3*^{-/-} *Irf5*^{-/-} *Irf7*^{-/-} TKO**
735 **mice. A-E.** WT, *Irf5*^{-/-}, and *Irf3*^{-/-} *Irf5*^{-/-} *Irf7*^{-/-} TKO mice were infected with 10⁶ FFU of OROV.
736 Four, 6, 9 or 12 days later, serum was collected and the levels of the indicated cytokines
737 were determined. Data points represent individual mice, and the bars indicate the mean
738 values ± standard deviations (SD). A blue cross indicates that all OROV-infected *Irf3*^{-/-} *Irf5*^{-/-}
739 *Irf7*^{-/-} TKO animals were dead at the indicated time point. The data corresponds to 4 to 13
740 mice per each group from two independent experiments. Asterisks indicate statistical
741 significance compared to serum from OROV-infected WT mice as judged by the Mann-
742 Whitney test (***, *P* < 0.001, ****, *P* < 0.0001). Dashed lines represent the mean values from
743 three mock-infected animals. **F.** WT and *Irf5*^{-/-} mice were infected with OROV and 1, 2, and 3
744 days later, the type I IFN activity in serum was measured by an EMCV inhibition bioassay.
745 Data are shown as the mean of 5 to 10 mice per group from two independent experiments
746 and asterisks represent statistical significance as determined by 2-way ANOVA (****, *P* <
747 0.0001).

748 **Figure 5. Analysis of liver tissue from OROV-infected WT, *Irf5*^{-/-}, and *Irf3*^{-/-} *Irf5*^{-/-}**
749 ***Irf7*^{-/-} TKO mice. A.** Histological (hematoxylin and eosin staining) analysis of the livers of
750 infected mice harvested 4 days after OROV infection **B.** Representative images of TUNEL
751 staining of livers of infected mice taken 4 days after OROV infection. **C.** Detection of OROV
752 antigen in liver of infected mice 4 days after virus infection. Images (20x magnification) were

753 obtained from one representative animal from groups of three. Inset images show a higher
754 magnification image (40x) and correspond to the region marked by the arrow. Scale bar =
755 100 μ m.

756 **Figure 6. Dying cells are present in the brains of OROV-infected *Irf5*^{-/-} mice.**

757 TUNEL analysis of the cerebral cortex (A), cerebellum (B), hippocampus (C) and midbrain
758 (D) from mice harvested 12 days after OROV infection. Representative images (10x
759 magnification) were obtained from three mice of each group. Inset images show a magnified
760 image and correspond to the region marked by the arrow. Scale bar = 100 μ m.

761 **Figure 7. OROV detection in the brains of *Irf5*^{-/-} mice after 12 days of infection.**

762 Immunohistochemical analysis after staining with polyclonal anti-OROV ascites fluid of the
763 cerebral cortex (A), cerebellum (B), hippocampus (C) and midbrain (D) from uninfected, WT,
764 and *Irf5*^{-/-} infected mice. Images are derived from one representative animal obtained from a
765 group of three animals. All sections were taken at 12 days of infection and the images were
766 obtained using a magnification of 20x. A higher resolution of infected cells is shown in the
767 inset with a higher magnification image (40x), corresponding to the region marked by the
768 arrow. Scale bar = 100 μ m.

769 **Figure 8. OROV RNA is detected in *Irf5*^{-/-} mice at later time points.** Viral burden

770 after OROV infection of WT and *Irf5*^{-/-} mice was determined by qRT-PCR in samples from
771 serum (A), liver (B), spleen (C), kidney (D), lung (E), brain (F), and spinal cord (G). Data
772 points represent individual mice. Bars indicate median values and were obtained from 6 to
773 13 mice per time point. Dashed lines represent the limit of sensitivity of the assay. Asterisks
774 indicate statistical significance as judged by the Mann-Whitney test (*, $P < 0.05$; **, $P < 0.01$;
775 ****, $P < 0.0001$).

776 **Figure 9. OROV induces less type I IFN production in circulating DC**

777 **populations from *Irf5*^{-/-} mice at late time points after OROV infection. A.** Cell isolation
778 scheme: CD3, CD19⁺, CD11b⁺, CD11c⁺ and B220⁺ cells were purified at day 8 after OROV
779 infection from WT and *Irf5*^{-/-} mice by positive selection using antibody-coated magnetic

780 beads. CD19⁺ cells were purified from the whole blood of 6 WT and *Irf5*^{-/-} mice and the CD3⁺
781 and CD11b⁺ were sequentially purified using the flow-through from CD19⁺ and CD3⁺ cells,
782 respectively. As CD19, CD3 and CD11b negative cells had detectable OROV RNA only in
783 *Irf5*^{-/-} mice, CD11c⁺ cells and B220⁺ cells subsequently were purified directly from whole
784 blood pooled of 5 WT and *Irf5*^{-/-} mice. **B.** Flow cytometry of the different cell populations
785 purified by positive selection showing the forward scatter (FSC) versus staining with the
786 specific antibody conjugated with FITC. The percentage of specific positive cells is showed
787 in the gate. **C.** Number of copies of OROV RNA per cell in the different cells populations as
788 determined by qRT-PCR after normalization to *Gapdh*. Each symbol indicates results from
789 pools of mice, following the scheme described above. **D.** Relative expression levels of *Irfnb*
790 mRNA as determined by qRT-PCR. Gene expression was normalized to *Gapdh* mRNA and
791 is shown as the fold increase compared to the cells from mock-infected mice on a log₂ scale.
792 The basal level of *Irfnb* mRNA was barely detectable and was similar in cells from WT and
793 *Irf5*^{-/-} mice. Data represent the averages from three independent experiments performed in
794 triplicate and are expressed as the means ± SD and asterisks indicate statistical significance
795 (*, *P* < 0.05) as determined by 2-way ANOVA. The dotted line represents the limit of
796 detection.

797 **Figure 10. OROV replicates in cultured DCs but not Mφ from *Irf5*^{-/-} mice.** Kinetics
798 of OROV replication in bone marrow-derived DCs (**A**) and Mφ (**B**) from WT, *Irf5*^{-/-}, and *Irf3*^{-/-}
799 *Irf5*^{-/-} *Irf7*^{-/-} TKO mice after infection at an MOI of 0.001. The data represent the mean ± SD of
800 three independent experiments performed in triplicate. All KO cell groups were compared to
801 WT by a two-way ANOVA, and asterisks indicate statistical significance (*, *P* < 0.05; **, *P* <
802 0.01; ***, *P* < 0.001). The dotted line represents the limit of detection of the assay. **C-F.**
803 Kinetics of *Irfna* (**C and E**) and *Irfnb* (**D and F**) expression in bone marrow-derived DCs (**C-D**)
804 and Mφ (**E-F**) from WT, *Irf5*^{-/-}, and *Irf3*^{-/-} *Irf5*^{-/-} *Irf7*^{-/-} TKO mice after infection with OROV using
805 an MOI of 0.001. The relative levels of *Irfna* and *Irfnb* mRNA were determined by qRT-PCR
806 after normalization to *Gapdh* mRNA, and are displayed as ΔΔCt values compared to the

807 mock-infected cells on a \log_2 scale. The basal level of *Irfna* and *Irfnb* mRNA was barely
808 detectable and was similar in cells from WT and *Irf5*^{-/-} mice. Data represent the averages
809 from three independent experiments performed in triplicate and are expressed as the means
810 \pm SD. The asterisks indicate statistical significance by two-way ANOVA (*, $P < 0.05$; **, $P <$
811 0.01) and the dotted line represents the limit of detection.

812 **Figure 11. The effect of IRF-5 on early antibody response in OROV-infected**
813 **mice. A-B.** Presence of neutralizing antibody in the serum from WT and *Irf5*^{-/-} mice at 8 (**A**)
814 and 12 (**B**) days after OROV infection as judged by a plaque reduction assay in Vero cells
815 after incubation with 100 PFU of OROV and \log_2 dilutions of the tested serum. Data in this
816 Figure represent the mean of 8 mice per group, from two independent experiments
817 performed in duplicate. All error bars represent the SD. The PRNT₅₀ represents the dilution
818 that showed 50% reduction in the number of plaque formation in comparison with a control
819 without serum after linear regression analysis.

820 **Figure 12. IRF-5 controls the neuropathogenesis of infection by LACV, a**
821 **related orthobunyavirus. A.** Survival analysis of eight week-old mice after inoculation with
822 10^5 FFU (n = 23 for WT, n = 17 for *Irf5*^{-/-}, n = 16 for *Irf3*^{-/-} *Irf7*^{-/-} DKO, n = 5 for *Irf3*^{-/-} *Irf5*^{-/-} *Irf7*^{-/-}
823 TKO) Asterisks indicate differences that were statistically significant compared to WT mice
824 by the log rank test (*, $P < 0.05$; ****, $P < 0.0001$). **B-D.** Weight loss analysis of eight week-
825 old mice after inoculation with 10^5 FFU of LACV by footpad inoculation in the same mice.
826 Data are pooled from at least two independent experiments. Survival curves were analyzed
827 by the log-rank test and weight loss was compared by 2-way ANOVA. Asterisks indicate
828 differences that were statistically significant compared to WT animals with the same viral
829 dose (*, $P < 0.05$; **, $P < 0.01$; ***, $P < 0.001$, ****, $P < 0.0001$). **F-G.** Viral burden after LACV
830 infection of WT or *Irf5*^{-/-} mice was determined by qRT-PCR in samples from brain (**F**) and
831 spinal cord (**G**). Data points represent individual mice. Bars indicate median values and were
832 obtained from 8 to 12 mice per time point. Dashed lines represent the limit of sensitivity of
833 the assay. Asterisks indicate statistical significance as judged by the Mann-Whitney test (*, P
834 < 0.05 ; **, $P < 0.01$).

835 **Table 1. Blood urea nitrogen (BUN), alkaline phosphatase (ALKP) and creatine kinase**
 836 **(CK) levels after OROV infection.**

837

Test	Genotype	4 dpi		6 dpi		9 dpi		12 dpi	
		U/L	P	U/L	P	U/L	P	U/L	P
BUN*	WT	22.5 ± 3.02	-	22.0 ± 3.4	-	19.0 ± 2.42	-	19.5 ± 3.88	-
	<i>Irf5</i> ^{-/-}	19.5 ± 7.27	0.10	14.0 ± 3.5	0.07	17.0 ± 3.3	0.34	21.5 ± 6.8	0.99
	TKO	19.0 ± 5.5	0.25	DEAD	-	DEAD	-	DEAD	-
ALKP	WT	144 ± 34.6	-	161 ± 41.0	-	177 ± 10.9	-	126 ± 30.3	-
	<i>Irf5</i> ^{-/-}	125 ± 31.3	0.26	134 ± 25.7	0.27	123 ± 21.6	0.09	151 ± 64.4	0.71
	TKO	103 ± 56.8	0.14	DEAD	-	DEAD	-	DEAD	-
CK	WT	5066 ± 1761	-	6657 ± 888	-	379.5 ± 171	-	551 ± 161	-
	<i>Irf5</i> ^{-/-}	6215 ± 585	0.46	6666 ± 999	0.26	3088 ± 820	0.05	3133 ± 998	0.05
	TKO	6478 ± 1315	0.92	DEAD	-	DEAD	-	DEAD	-

838

839 WT, *Irf5*^{-/-} or *Irf3*^{-/-} *Irf5*^{-/-} *Irf7*^{-/-} (TKO) indicated mice were inoculated with OROV. Serum was
 840 collected at 4, 6, 9 and 12 days after infection, and blood chemistry were measured by Bio-
 841 Plex array. Data represent the median ± SD in U/L of 5 to 11 mice per group. Statistical
 842 significance was determined using the Mann-Whitney test and *P* values were obtained after
 843 comparison to WT mice infected in parallel. * BUN and was quantified in mg/dl.

844

845
846**Table 2. Serum cytokine and chemokine levels after OROV infection**

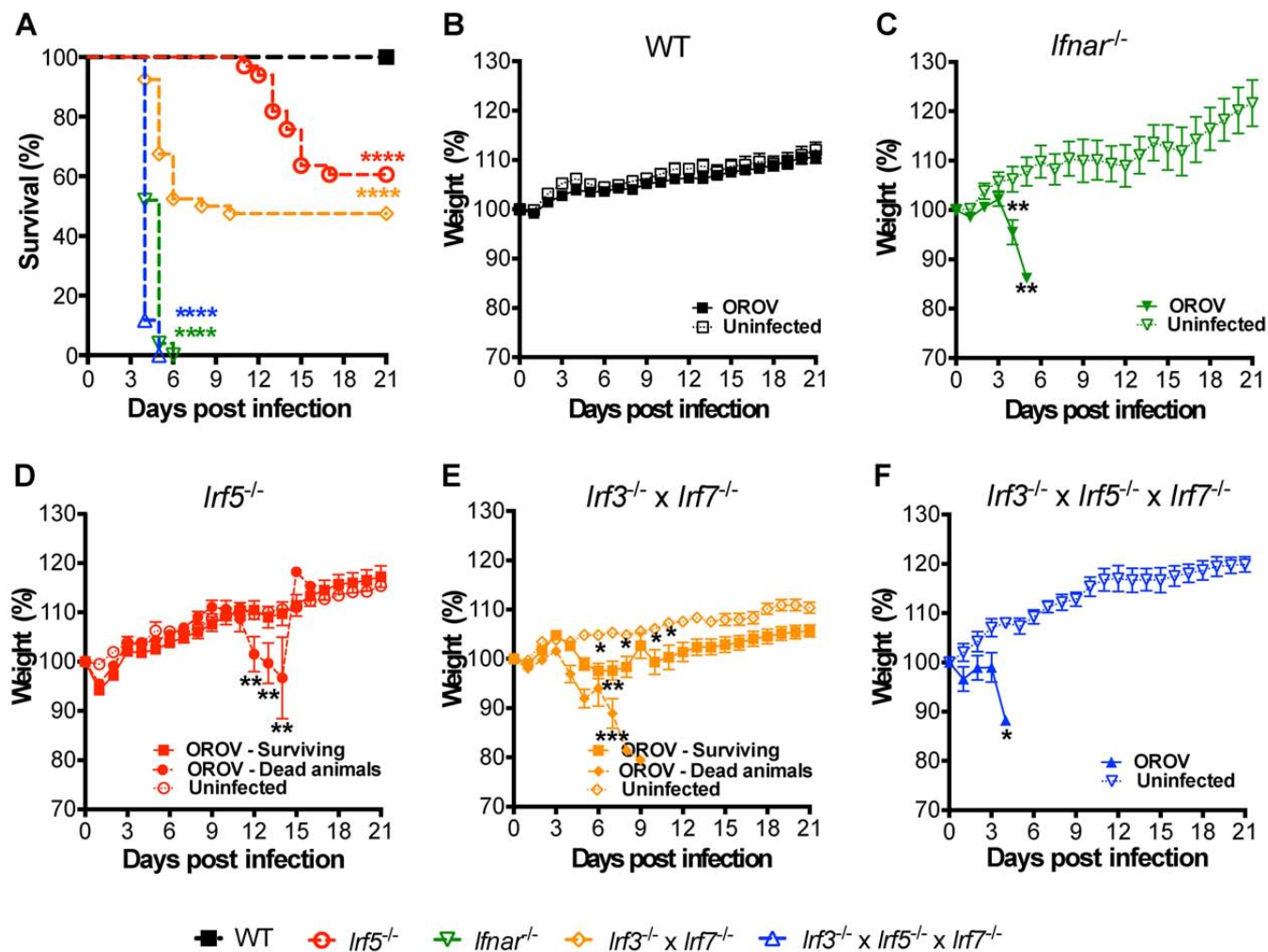
Cytokine	Genotype	4 dpi		6 dpi		9 dpi		12 dpi	
		pg/ml	P	pg/ml	P	pg/ml	P	pg/ml	P
IL-1 α	WT	1.0 \pm 1.58	-	3.6 \pm 2.3	-	1.2 \pm 2.1	-	0.8 \pm 1.8	-
	<i>Irf5</i> ^{-/-}	2.5 \pm 4.3	0.56	2.5 \pm 7.9	0.84	3.4 \pm 4.1	0.69	2.1 \pm 5.1	0.51
	TKO	0.0 \pm 12.8	0.57	DEAD	-	DEAD	-	DEAD	-
IL-1 β	WT	199 \pm 44	-	200 \pm 53	-	192 \pm 24	-	180 \pm 18	-
	<i>Irf5</i> ^{-/-}	260 \pm 156	0.22	145 \pm 294	0.71	188 \pm 74	0.89	225 \pm 123	0.64
	TKO	175 \pm 138	0.53	DEAD	-	DEAD	-	DEAD	-
IL-2	WT	18.3 \pm 14.6	-	17.5 \pm 21.9	-	16.7 \pm 11.4	-	17.8 \pm 9.0	-
	<i>Irf5</i> ^{-/-}	50.1 \pm 39.1	0.32	43.1 \pm 77.3	0.26	22.8 \pm 11.5	0.78	11.5 \pm 11.2	0.41
	TKO	7.0 \pm 19.3	0.02	DEAD	-	DEAD	-	DEAD	-
IL-3	WT	7.5 \pm 11.9	-	16.4 \pm 13.2	-	21.5 \pm 6.1	-	26.1 \pm 8.9	-
	<i>Irf5</i> ^{-/-}	7.8 \pm 4.3	0.50	6.9 \pm 7.1	0.29	39.9 \pm 21.8	0.38	36.2 \pm 19.2	0.52
	TKO	6.9 \pm 19.2	0.82	DEAD	-	DEAD	-	DEAD	-
IL-4	WT	0.0 \pm 8.3	-	7.5 \pm 9.0	-	14.2 \pm 5.8	-	15.9 \pm 6.5	-
	<i>Irf5</i> ^{-/-}	0.0 \pm 4.8	0.42	0.0 \pm 2.6	0.17	24.0 \pm 12.6	0.29	22.7 \pm 11.3	0.45
	TKO	0.0 \pm 1.3	0.41	DEAD	-	DEAD	-	DEAD	-
IL-5	WT	15.0 \pm 7.5	-	17.4 \pm 7.1	-	22.9 \pm 5.1	-	21.6 \pm 4.9	-
	<i>Irf5</i> ^{-/-}	20.0 \pm 10.0	0.75	19.2 \pm 19.8	0.76	25.3 \pm 13.1	0.41	11.3 \pm 10.5	0.62
	TKO	8.7 \pm 4.3	0.06	DEAD	-	DEAD	-	DEAD	-
IL-6	WT	4.5 \pm 1.5	-	5.0 \pm 2.9	-	4.2 \pm 0.9	-	4.7 \pm 1.3	-
	<i>Irf5</i> ^{-/-}	8.9 \pm 6.0	0.17	4.5 \pm 7.8	0.55	6.9 \pm 2.9	0.07	6.1 \pm 3.9	0.9
	TKO	100 \pm 301	<0.0001	DEAD	-	DEAD	-	DEAD	-
IL-9	WT	117 \pm 115	-	68 \pm 131	-	0.0 \pm 7.9	-	0.0 \pm 16.9	-
	<i>Irf5</i> ^{-/-}	213 \pm 237	0.35	0.0 \pm 143	0.49	0.0 \pm 0.0	0.99	0.0 \pm 0.0	0.99
	TKO	0.0 \pm 96	0.24	DEAD	-	DEAD	-	DEAD	-
IL-10	WT	20.8 \pm 16.3	-	24.5 \pm 14.4	-	20.1 \pm 11.7	-	21.7 \pm 7.0	-
	<i>Irf5</i> ^{-/-}	53.5 \pm 27.7	0.17	57.0 \pm 44.6	0.30	34.3 \pm 17.6	0.78	28.1 \pm 16.9	0.9
	TKO	10.0 \pm 27.9	0.58	DEAD	-	DEAD	-	DEAD	-
IL-12 (p40)	WT	29.3 \pm 30.9	-	29.8 \pm 17.6	-	19.5 \pm 1.5	-	22.2 \pm 7.5	-
	<i>Irf5</i> ^{-/-}	27.8 \pm 5.9	0.51	32.0 \pm 16.5	0.71	31.0 \pm 11.5	0.06	22.6 \pm 10.0	0.87
	TKO	191 \pm 125	<0.0001	DEAD	-	DEAD	-	DEAD	-
IL-12 (p70)	WT	23.9 \pm 12.2	-	24.8 \pm 8.8	-	22.8 \pm 2.2	-	23.6 \pm 4.3	-
	<i>Irf5</i> ^{-/-}	33.8 \pm 17.9	0.23	26.8 \pm 25.6	0.85	53.6 \pm 28.5	0.38	49.5 \pm 27.5	0.64
	TKO	22.6 \pm 13.9	0.98	DEAD	-	DEAD	-	DEAD	-
IL-13	WT	28.8 \pm 26.2	-	45.8 \pm 52.1	-	26.5 \pm 38.2	-	35.4 \pm 11.5	-
	<i>Irf5</i> ^{-/-}	89.8 \pm 281.4	0.054	216 \pm 330	0.19	25.2 \pm 23.8	0.66	11.5 \pm 26.4	0.62
	TKO	13.4 \pm 62.0	0.30	DEAD	-	DEAD	-	DEAD	-
IL-17	WT	5.6 \pm 5.1	-	8.7 \pm 6.6	-	12.8 \pm 3.2	-	13.2 \pm 4.1	-
	<i>Irf5</i> ^{-/-}	7.6 \pm 4.0	0.87	5.8 \pm 5.4	0.53	23.1 \pm 14.8	0.37	20.4 \pm 11.8	0.64
	TKO	7.5 \pm 5.3	0.91	DEAD	-	DEAD	-	DEAD	-
Eotaxin	WT	455 \pm 287	-	502 \pm 230	-	513 \pm 135	-	454 \pm 221	-
	<i>Irf5</i> ^{-/-}	527 \pm 413	0.87	512 \pm 796	0.94	559 \pm 517	0.89	281 \pm 490	0.62
	TKO	30.9 \pm 221	0.02	DEAD	-	DEAD	-	DEAD	-
G-CSF	WT	15.9 \pm 5.2	-	14.8 \pm 5.5	-	15.0 \pm 1.8	-	18.1 \pm 4.2	-
	<i>Irf5</i> ^{-/-}	15.9 \pm 30.0	0.94	9.6 \pm 13.6	0.47	29.9 \pm 22.5	0.38	19.3 \pm 14.0	0.77
	TKO	1499 \pm 2899	<0.0001	DEAD	-	DEAD	-	DEAD	-

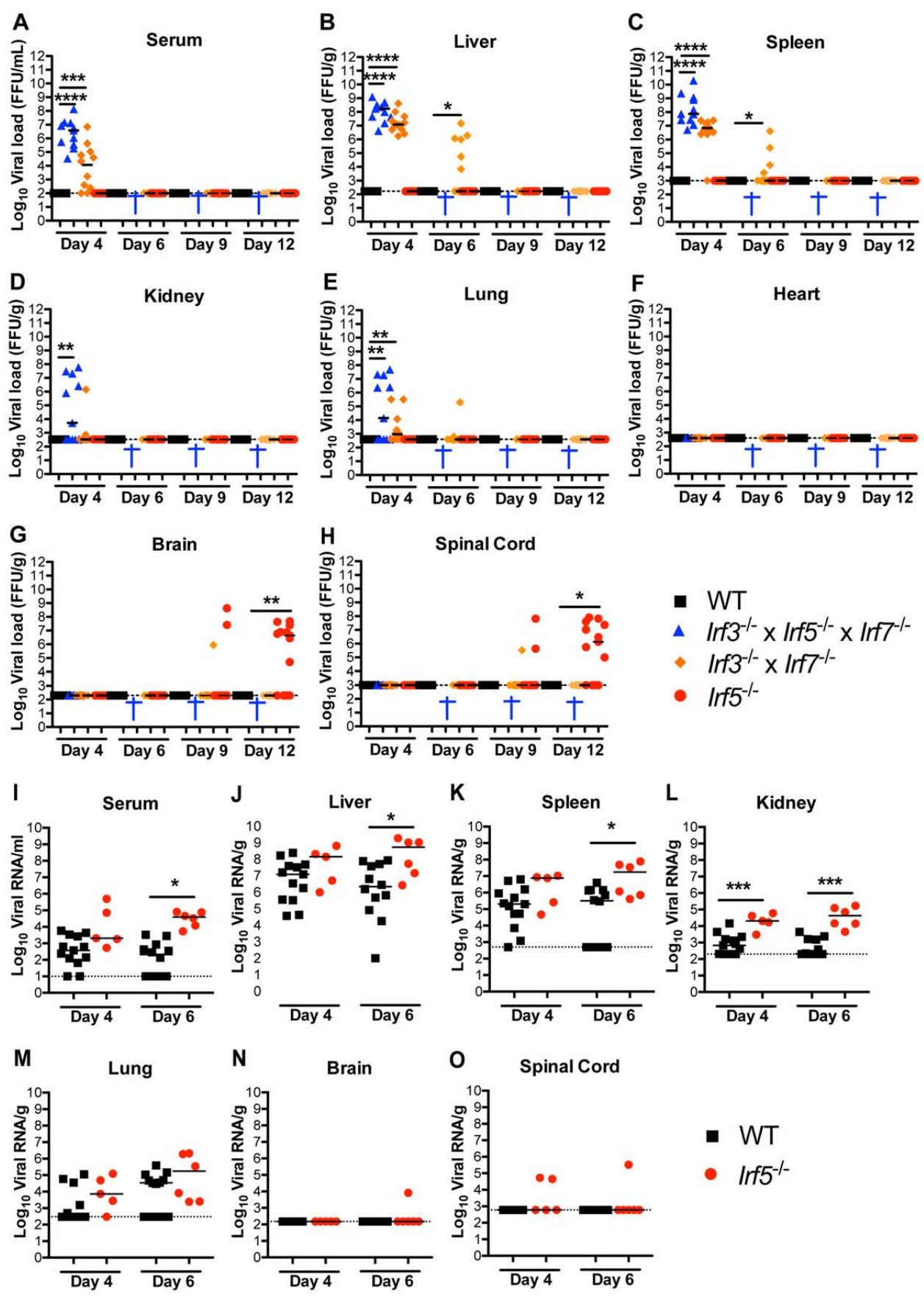
GM-CSF	WT	64.4 ± 26.6	-	75.9 ± 29.3	-	94.9 ± 15.7	-	93.8 ± 24.0	-
	<i>Irf5</i> ^{-/-}	60.6 ± 37.9	0.47	35.5 ± 61.3	0.34	109.9 ± 66.4	0.77	106.8 ± 62	0.64
	TKO	39.8 ± 30.3	0.16	DEAD	-	DEAD	-	DEAD	-
IFN-γ	WT	2.1 ± 2.1	-	2.4 ± 1.4	-	1.9 ± 0.5	-	1.6 ± 0.7	-
	<i>Irf5</i> ^{-/-}	4.7 ± 2.7	0.34	3.4 ± 7.5	0.76	2.1 ± 0.8	0.29	1.6 ± 1.8	0.9
	TKO	2.1 ± 3.1	0.97	DEAD	-	DEAD	-	DEAD	-
KC	WT	30.0 ± 9.6	-	31.1 ± 19.7	-	23.0 ± 2.8	-	27.3 ± 7.8	-
	<i>Irf5</i> ^{-/-}	24.4 ± 42	0.87	24.3 ± 14.5	0.24	37.7 ± 20.8	0.07	19.8 ± 9.3	0.87
	TKO	151 ± 465	<0.0001	DEAD	-	DEAD	-	DEAD	-
MCP-1	WT	226 ± 113	-	237 ± 132	-	252 ± 59	-	222 ± 61	-
	<i>Irf5</i> ^{-/-}	252 ± 141	0.42	279 ± 235	0.59	300 ± 219	0.99	134 ± 230	0.62
	TKO	146 ± 273	0.92	DEAD	-	DEAD	-	DEAD	-
MIP-1α	WT	1.8 ± 1.4	-	2.2 ± 1.8	-	2.6 ± 1.3	-	2.8 ± 1.4	-
	<i>Irf5</i> ^{-/-}	0.5 ± 0.7	0.18	2.4 ± 6.4	0.84	4.7 ± 2.6	0.3	3.2 ± 2.2	0.92
	TKO	13.1 ± 9.7	0.0016	DEAD	-	DEAD	-	DEAD	-
MIP-1β	WT	38.5 ± 22.4	-	47.7 ± 20.4	-	53.1 ± 6.6	-	55.0 ± 10.0	-
	<i>Irf5</i> ^{-/-}	34.0 ± 20.1	0.51	44.6 ± 29.7	0.79	71.0 ± 40.2	0.36	76.9 ± 38.7	0.62
	TKO	14.4 ± 10.6	0.02	DEAD	-	DEAD	-	DEAD	-
RANTES	WT	15.1 ± 5.8	-	14.9 ± 5.1	-	14.5 ± 1.2	-	16.1 ± 2.3	-
	<i>Irf5</i> ^{-/-}	16.7 ± 1.7	0.27	16.6 ± 18.2	0.76	29.7 ± 16.0	0.38	25.8 ± 14.3	0.64
	TKO	20.3 ± 15.1	0.01	DEAD	-	DEAD	-	DEAD	-
TNF-α	WT	271 ± 193	-	370 ± 182	-	425 ± 65	-	451 ± 111	-
	<i>Irf5</i> ^{-/-}	358 ± 198	0.97	230 ± 307	0.47	621 ± 354	0.38	596 ± 347	0.64
	TKO	130 ± 302	0.36	DEAD	-	DEAD	-	DEAD	-

847
848

849 WT, *Irf5*^{-/-} or *Irf3*^{-/-} *Irf5*^{-/-} *Irf7*^{-/-} (TKO) mice were inoculated with OROV. Serum was collected
850 at days 4, 6, 9 and 12 after infection, and cytokines and chemokines were measured by Bio-
851 Plex array. Data represent the median ± SD in pg/ml of 5 to 11 mice per group. Statistical
852 significance was determined using the Mann-Whitney test, and *P* values were obtained after
853 comparison to WT mice infected in parallel.

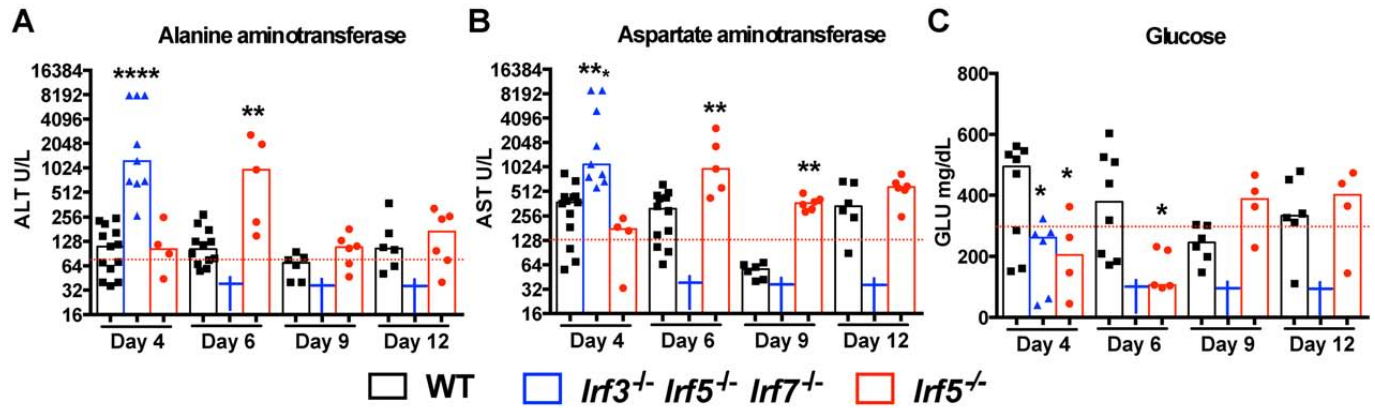
854

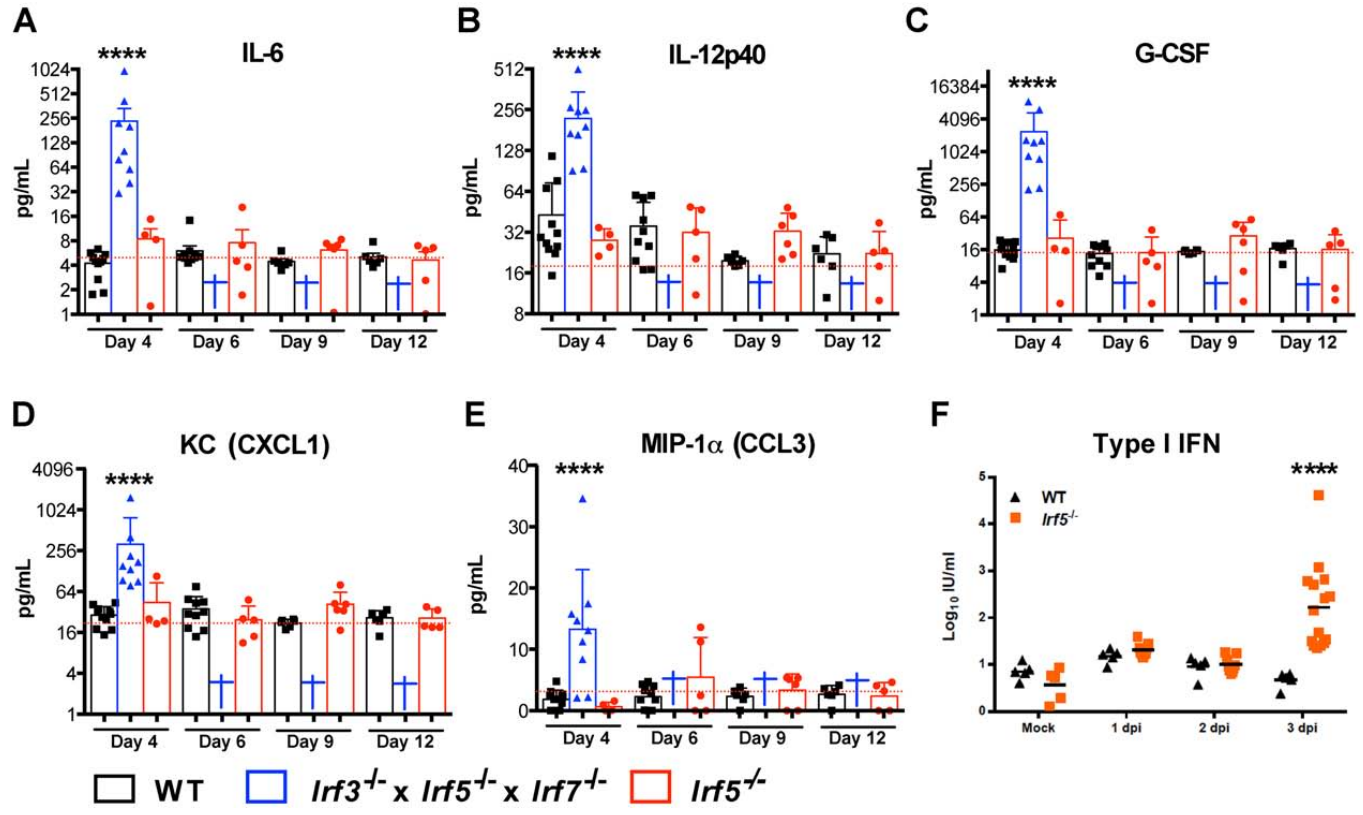


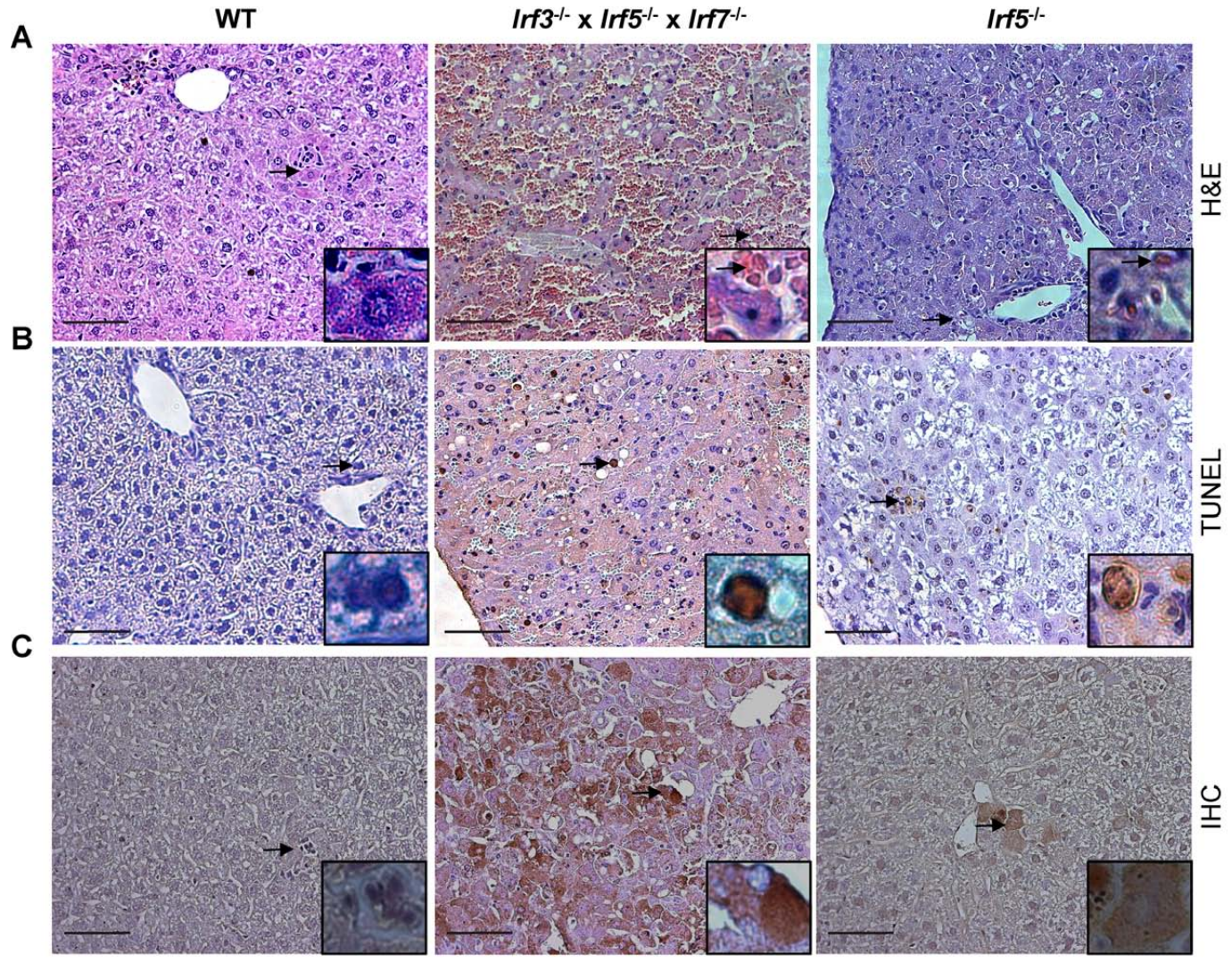


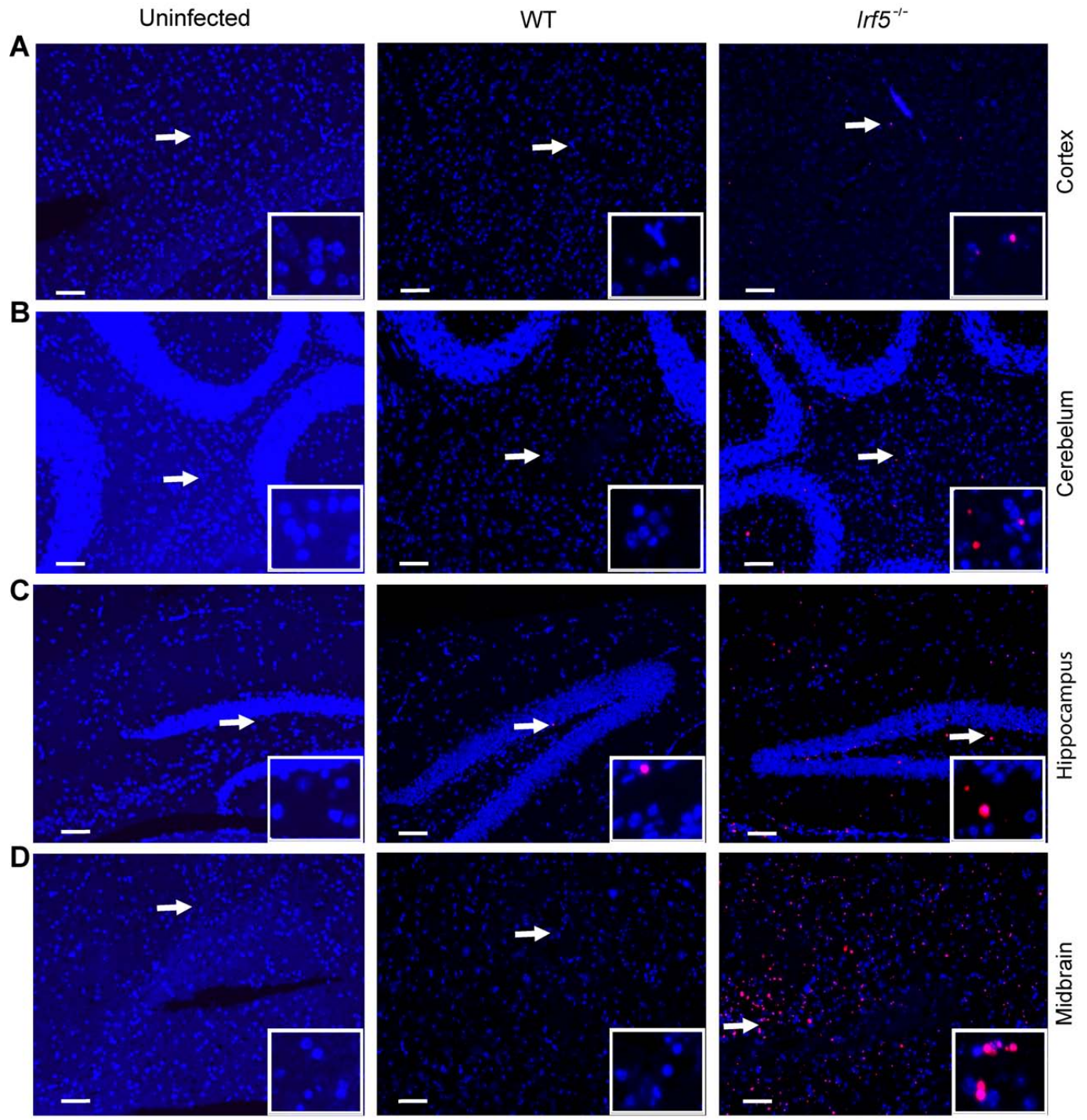
FOCUS FORMING ASSAY

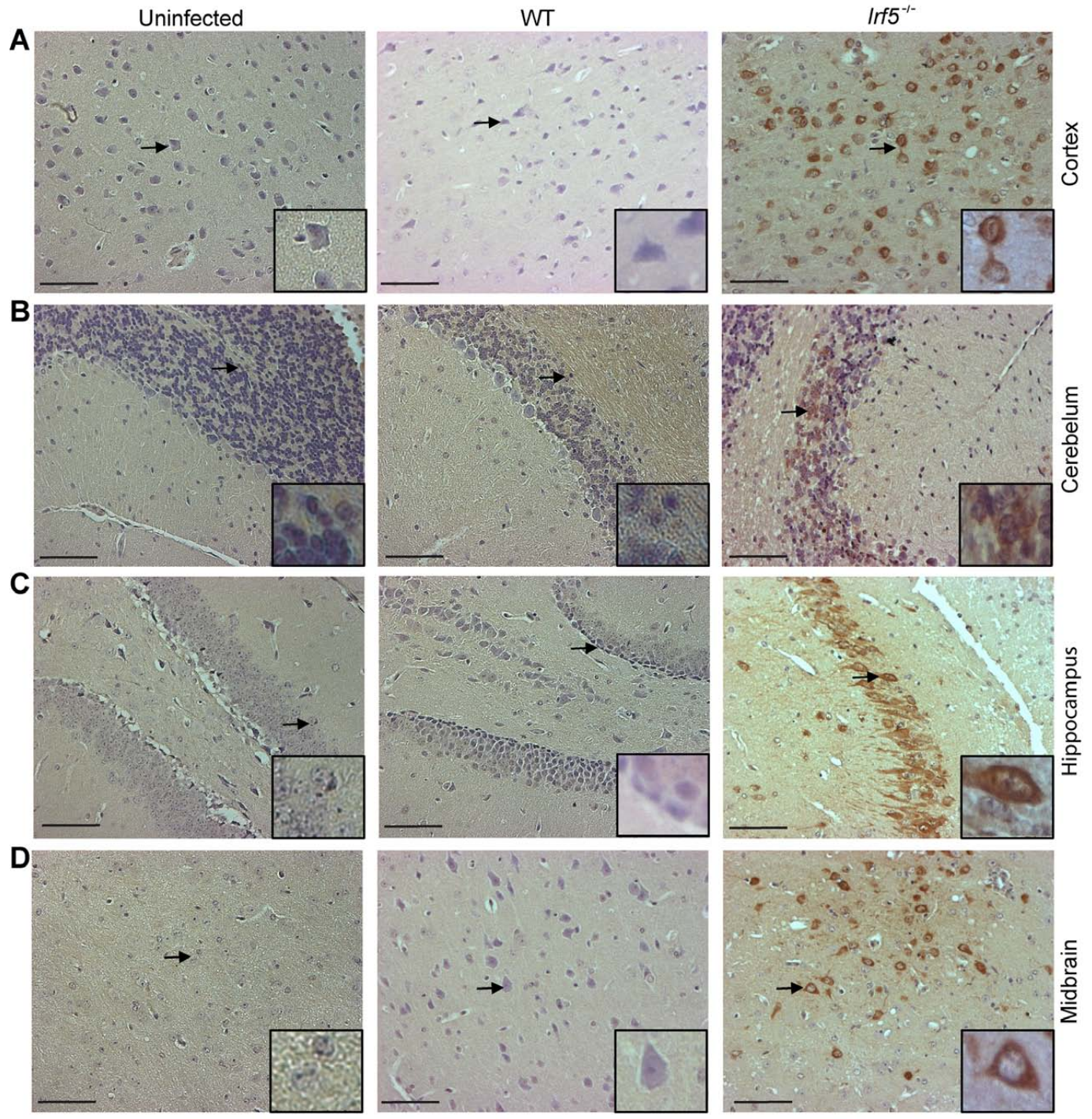
qRT-PCR

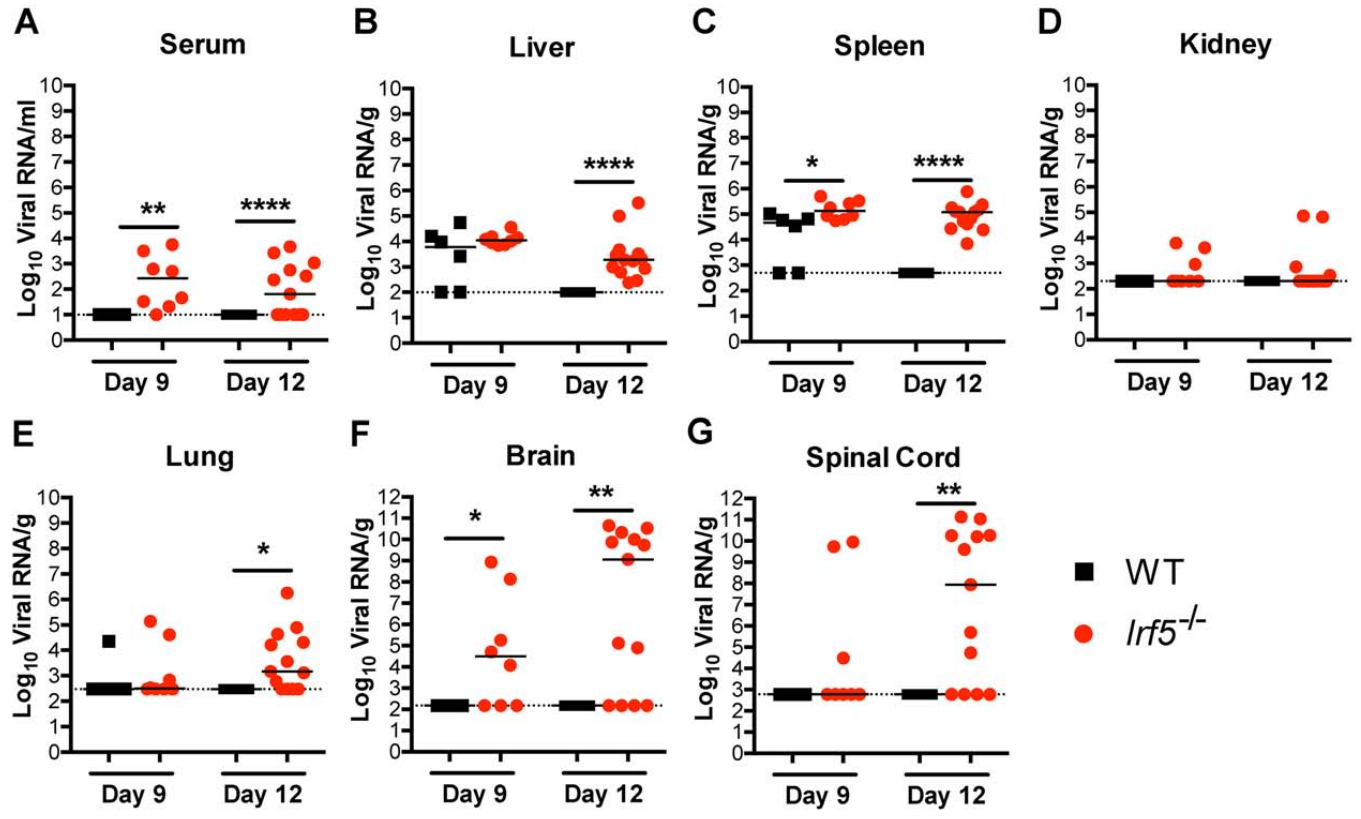


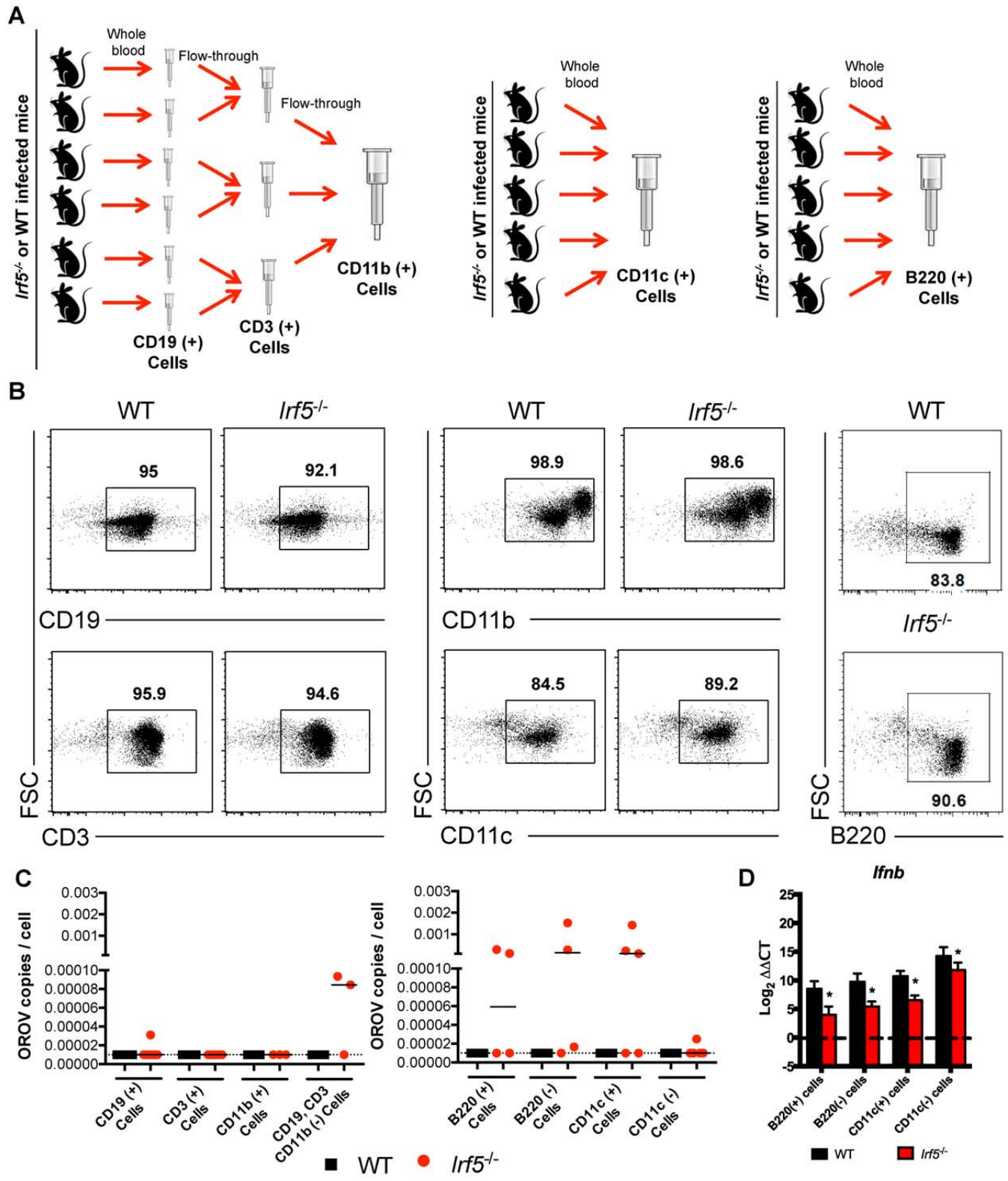


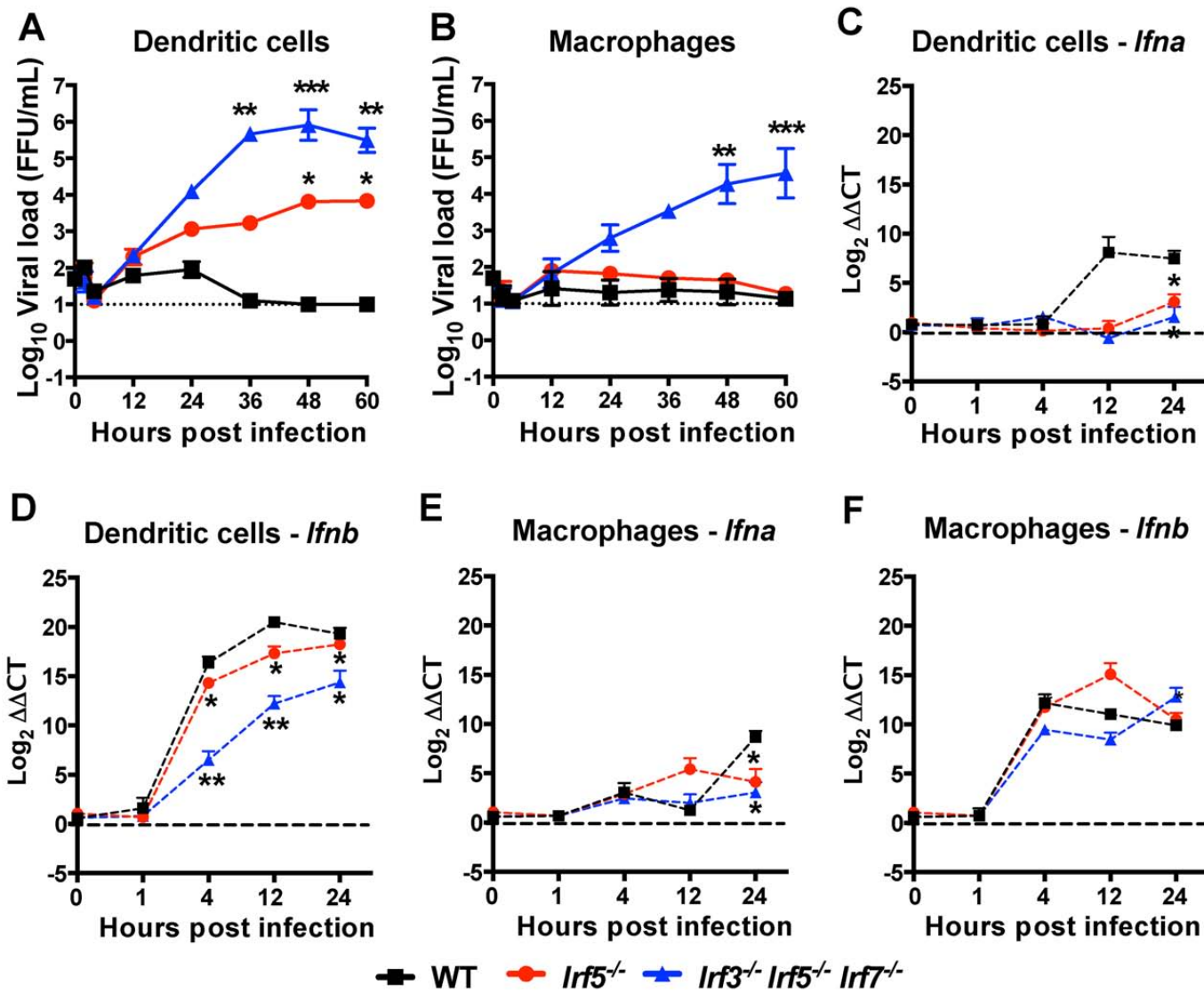


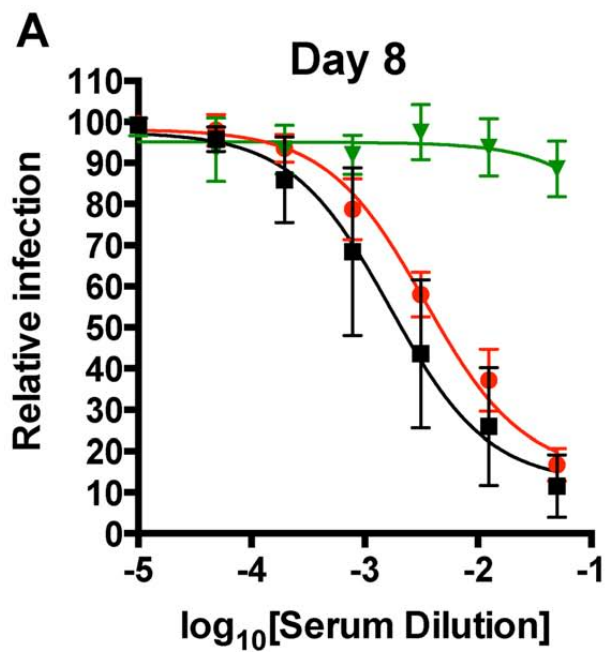




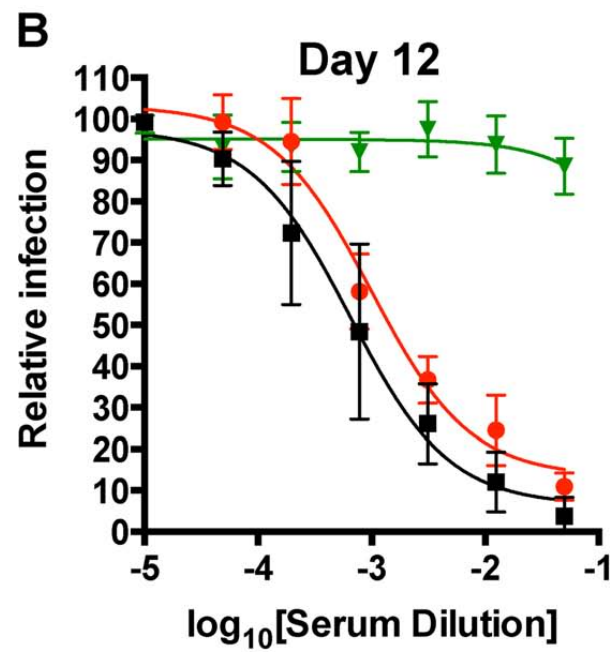








- WT (PRNT₅₀ ≥ 1:600)
- Irf5^{-/-} (PRNT₅₀ ≥ 1:300)
- ▼ Naive Serum (PRNT₅₀ > 1:20)



- WT (PRNT₅₀ ≥ 1:1550)
- Irf5^{-/-} (PRNT₅₀ ≥ 1:1000)
- ▼ Naive Serum (PRNT₅₀ > 1:20)

